Phenomenology and Dynamics of Competitive Ecosystems Beyond the Niche-Neutral Regimes

Nava Leibovich and Jeremy Rothschild
Department of Physics, University of Toronto

Sidhartha Goyal* and Anton Zilman†
Department of Physics, University of Toronto   and
Institute for Biomedical Engineering, University of Toronto

Structure, composition and stability of ecological populations are shaped by the inter- and intra-species interactions within these communities. It remains to be fully understood how the interplay of these interactions with other factors, such as immigration, control the structure, diversity and the long term stability of ecological systems in the presence of noise and fluctuations. We address this problem using a minimal model of interacting multi-species ecological communities that incorporates competition, immigration and demographic noise. We find that the complete phase diagram exhibits rich behavior with multiple regimes that go beyond the classical 'niche' and 'neutral' regimes, extending and modifying the 'neutral-like' or 'niche-like' dichotomy. In particular, we observe novel regimes that cannot be characterized as either 'niche' or 'neutral' where a multimodal species abundance distribution is observed. We characterize the transitions between the different regimes and show how they arise from the underlying kinetics of the species turnover, extinction and invasion. Our model serves as a minimal null model of noisy competitive ecological systems, against which more complex models that include factors such as mutations and environmental noise can be compared.

I. INTRODUCTION

Composition and behavior of ecological communities are shaped by direct and indirect interactions between the species of these communities, such as the competition for the physical space and the intrinsic and the extrinsic resources. The examples of such competitive ecosystems are microbial communities in various biomes such as the soil [1], the ocean [2, 3] and the human body [4] - in particular the human gut which hosts a diverse microbiome whose dynamics are important for human health [5, 6]. In the context of cellular populations within organisms, the evolution of neoplasms and tumor cells [7–9], interactions within the immune system [10, 11], as well as the appearance of dominant clones during cell reprogramming [12], exhibit phenomenology akin to ecological competition. Beyond biology [13–15], competitive interactions shape behaviors in a vast array of systems such as competition economics [16] and social networks [17].

A classical example of the effects of inter-species competition - which inspired important ecological competition paradigms - is the differentiation in beak forms of finches in the Galápagos islands [18, 19]. On these islands, dissimilar finch species possess beaks of varying shapes and sizes allowing them to consume different food sources and thus occupy distinct niches; this type of ecosystem structure is commonly referred to as an ecological niche model [20, 21]. Various niche models have been used to describe the community structures observed in diverse ecosystems such as plant grassland communities [22, 23], marine plankton [24] and conservation ecology [25, 26]. Commonly, niche specialization results in weaker competition for resources between individuals occupying separate niches (inter-species competition) compared to the competition between individuals of the same kind residing in the same niche (intra-species competition). The competition strength (determining the niche overlap [27, 28]) defined as the ratio between the inter-specific and intra-specific competition strengths.

Another paradigmatic class of ecological models comprises neutral models that are often used to describe noisy ecosystems wherein individuals from distinct species are functionally equivalent. In contrast to niche models, interactions between all individuals in neutral models are identical regardless of their species [29–31]. Thus, neutral models have commonly served as the null hypotheses for the exploration of ecological processes in various settings where the differences between inter-specific and intra-specific interaction are functionally negligible [29, 32, 33]. Neutral theories can be viewed as a limit of niche theories where inter-specific and intra-specific interactions are equal: in other words, all species reside in completely overlapping niches [21, 34, 35].

In multi-species communities, the intra- and inter-species interactions as well as interactions with the environment, can lead to complex community composition and population dynamics; some species survive in the long term, while others are driven to extinction. However, in large communities with high numbers of competing species, it is often impractical or impossible to characterize the entire system composition by the assemblage of abundances for each species. Hence, coarse-grained paradigmatic descriptions are often used to provide gen-

---

* goyal@physics.utoronto.ca
† zilmana@physics.utoronto.ca

eral insights into the common behavior of these ecological communities.

Two variables commonly used to characterize complex ecological communities are 1) the richness, reflecting the number of co-occurring species [36, 37], and 2) the species abundance distributions (SAD) - the number of species present at a given abundance. The latter is closely related to the species rank abundance (SRA) - the species ranked in terms of their abundance [38–42]. These aggregate variables are observable experimentally and serve as the reporters on the underlying community structure, dynamics and the interaction network [43–46]. Richness, for example, is commonly considered to be an indicator of the competition strength and stability of the ecosystem [47–51].

The shape of the SAD is also used as a proxy for the structure of the underlying interactions' network. For high immigration or weak inter-species competition, the SAD commonly has a peak at high species abundance, away from extinction. This community structure is closely related to the niche models whereby different species co-exist: most species inhabit their own niches with their species abundance fluctuating around the peak of the SAD. Conversely, other ecosystems, such as many microbial communities and T-cell repertoires, exhibit few high-abundance species alongside highly diverse populations of low-abundance species [40, 52]. This 'rare biosphere' or 'hollow-curved distribution' is described by a unimodal, monotonically decreasing SAD. Interestingly, this unimodal behaviour is empirically observed in many different ecosystems and is often considered universal (see [53] and references therein). Neutral models have been championed to describe the emergence of this universality, although other theoretical explanations for the 'rare biosphere' SAD in competitive ecosystems have been suggested [41, 54].

Many theoretical studies that have aimed to quantify the competitive dynamics, the richness and the abundance distributions in ecological populations applied to various systems, commonly employ a small number of paragidmatic models. One common model of ecological competition is the deterministic, competitive Lotka-Voltera (LV) model, which has been especially useful in characterizing the niche regime by describing stable species coexistence as stable fixed points of the model. Depending on the ratios of inter- and intra-species competition strengths, deterministic LV models provide examples of both the 'niche-like' regimes of multiple species coexistence, and the competitive exclusion where species with weaker intra-species interactions drive others to extinction [55–58]. In complex scenarios, such as when the strengths of inter-specific interactions are randomly distributed among different species pairs, multi-species deterministic LV models can exhibit not only deterministic fixed point coexistence but also chaotic behavior reflected in the SAD shapes and richness [59–63]. Beyond disorder in the interaction network, dynamical noise from various sources - both extrinsic and intrinsic - can have impor-

tant effects on the system composition and dynamics, especially in the neutral regime. In order to capture experimentally observed stochastic fluctuations of population abundances, environmental noise is often introduced into the mathematical models [52, 64–67]. In particular, by tuning the strength of environmental noise the shape of the SAD can change from unimodal to bimodal [64], indicating a transition between 'niche-like' and 'neutral-like' regimes.

Regardless of the presence of the external environmental noise or randomness in the interaction network, the demographic noise - the inherent randomness of birth and death events - is ever-present and has fundamental impact on the community structure and stochastic population dynamics [30, 68, 69]. In particular, demographic noise has been suggested to be responsible for the SAD shape in neutral systems; these are characterized by the power law decay with an exponential cutoff that may account for 'rare biosphere' abundance and distributions observed in many experimental systems [30, 70, 71]. On the other hand, birth-death-immigration processes with demographic noise have also been shown to exhibit bimodal SADs at very low immigration rates [72] breaking from the paradigm wherein neutrality is synonymous to an SAD of 'rare biosphere' type. Although demographic noise models have been shown to reproduce observed features of a number of ecological systems [28, 51, 69, 73], a complete picture of the different regimes of community structures, is still missing. In particular, it remains to be fully understood how the interplay of the competition strength, the immigration rate, demographic noise and the resulting dynamics of species turnover shape transitions between these different community structure regimes.

In this paper, we systematically study the full parameter space of the community composition and structure using a competitive LV model with the demographic noise and an interaction network of minimal complexity; more complex scenarios may be examined by building on this paradigmatic null model. We show that, beyond the perception of dichotomous neutral-niche regimes, many different regimes of richness and shape of the abundance distribution emerge from the interplay between the competition strength and immigration in the presence of stochasticity as illustrated in Fig. 1). These regimes exhibit contrasting dynamics that underpin the differences in the community structures in different regimes, and the transitions between them.

The paper is structured as follows. In Sec. II we introduce the minimal model. In Sec. III we present our main results, including the regimes boundaries, their richness and the abundance distributions, as well as their associated underlying dynamics, and the species correlation structure. Lastly, in Sec. IV, we discuss our results in the context of experimental observations.
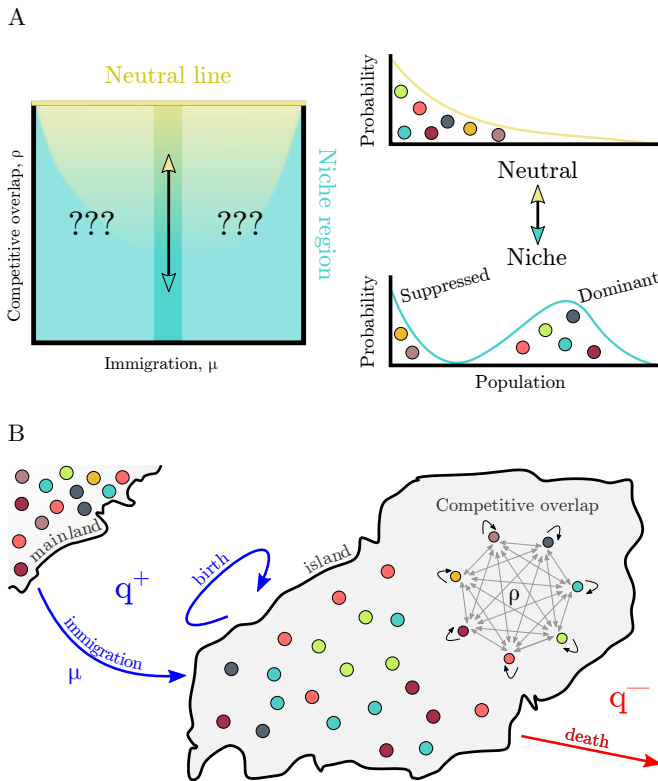
FIG. 1. Island model. Panel A: Conventionally, weak competition is associated with 'niche-like' bimodal SAD, while strong competition is linked to 'neutral-like' monotonously decreasing SAD. However, this paradigm is not complete, since the dependence on other parameters, such as immigration rate μ or diversity S, is not fully investigated. Thus, the entire phase space, e.g. (μ, ρ) or (S, ρ), remains unexplored. Panel B: The model illustration. An island with J individuals from S^* species. Each individual may proliferate and die with some rate corresponding to inter- and intraspecific interactions within the island. Here we consider deterministic, symmetric, fully-connected interspecific interactions network, governed by single parameter; the competitive overlap ρ. Additionally, individuals may migrate from a cloud/mainland, contains S species, into the island with a constant rate μ.

II. MATHEMATICAL MODELS AND METHODS

The minimal model studied in this paper incorporates three essential features of the ecological processes: competitive interactions, immigration and intrinsic demographic noise [69, 74]. In the model, illustrated in Fig. 1B, the community composition is characterized by the species abundances, $\vec{n} = (n_1, \ldots n_i \ldots n_S)$ where the discrete random variable n_i represents the number of individuals of the i-th species, and S is the total number of species. The dynamics of the system are described by a birth-death process with interactions, whereby the abundance (number of individuals) of any species can increase by one with the birth rate q^+ or decrease by one with the

death rate q^- defined as

$$q_i^+(\vec{n}) = r^+ n_i + \mu, \tag{1}$$

$$q_i^-(\vec{n}) = r^- n_i + \frac{r}{K} n_i \left(n_i + \sum_{j \neq i} \rho_{j,i} n_j \right)$$

for each species $i \in \{1, 2, \ldots, S\}$.

The birth rate incorporates two factors: the per-capita birth rate r^+ corresponding to procreation, and the constant and positive immigration rate μ from an external basin which ensures that the system possesses no global absorbing extinction state [28]. The death rates include the 'bare' per-capita death rate of the organisms r^- and the competitive interactions effects that increase the mortality at high population numbers, incorporated through a quadratic term in the death rates; Parameter $\rho_{j,i}$ quantifies the competition strength between species i and j. The carrying capacity for each species is represented by K. The per-capita turnover rate is $r = r^+ - r^-$.

These aggregate coarse-grained parameters are determined by a variety of system factors such as the efficiency of resource consumption, interactions with the environment and external forces. Although it is possible to derive these rates from explicit resource competition models in several special cases, the expressions are highly model-dependent and are not explicitly modeled here [75–77]. For biological reasons, K, r^+, $r^- > 0$ are all positive, which results in strictly positive transition rates for all $n_i \geq 0$. In this paper, we focus on the homogeneous case where the parameters (μ, K, ρ, r^+, and r^-) are identical for all species and the competitive interactions $\forall i, j : \rho_{j,i} = \rho$ for all species pairs. This symmetric and homogeneous interaction network has been used in [27, 51, 69, 73] in contrast to the models wherein the competition strengths are inhomogeneous and drawn from a distribution [64, 78]. This minimal complexity model allows us to investigate the full phase space of the system to examine the underlying principle without impractical multi-parameter sweeps.

The stochastic evolution of the system is described by the master equation

$$\partial_t \mathcal{P}(\vec{n}; t) = \sum_i \left\{ - \left[q_i^+(\vec{n}) + q_i^-(\vec{n}) \right] \mathcal{P}(\vec{n}; t) \right.$$
$$\left. + q_i^+(\vec{n} - \vec{e}_i) \mathcal{P}(\vec{n} - \vec{e}_i; t) + q_i^-(\vec{n} + \vec{e}_i) \mathcal{P}(\vec{n} + \vec{e}_i; t) \right\}, \tag{2}$$

where $\vec{e}_i$ is the standard basis vector and $\mathcal{P}(\vec{n}, t)$ is the joint probability density function for the system to exhibit the species composition $\vec{n}$ at time t [79]. In the long time limit, the system reaches a stationary state where $\partial_t \mathcal{P} = 0$.

The species abundance distribution (SAD) describing the mean fractions of species with n individuals, can be related to the marginal single species probability distri-

bution $P(n)$:

$$\text{SAD}(n) = \frac{1}{S}\left\langle \sum_{i=1}^{S} \delta(n_i - n)\right\rangle \tag{3}$$

$$= \frac{1}{S}\sum_{i=1}^{S}\left[\sum_{n_1=0}^{\infty}\cdots\sum_{n_{i-1}=0}^{\infty}\sum_{n_{i+1}=0}^{\infty}\cdots\sum_{n_S=0}^{\infty}\mathcal{P}(\vec{n})|_{n_i=n}\right]$$

$$= P_i(n) \equiv P(n),$$

where δ is the Kronecker delta function, and using the fact that in this homogeneous system the marginal distributions $P_i(n) = P(n)$ of population abundance are identical for all species.

In the Fokker-Planck approximation, the continuous deterministic limit of the master equation (2) recovers the well-known competitive Lotka-Volterra (LV) equations

$$\frac{\partial x_i}{\partial t} = q_i^+(\vec{x}) - q_i^-(\vec{x})$$

$$= rx_i\left(1 - \frac{x_i}{K} + \sum_{j\neq i}\rho\frac{x_j}{K}\right) + \mu \tag{4}$$

for the variable x_i, which corresponds to the continuous deterministic limit of the discrete variable n_i [79]; see Supplementary Materials (SM) for further details.

The deterministic steady state is given by

$$\tilde{x}(S) = \frac{K}{2[1+\rho(S-1)]}\left\{1 + \sqrt{1 + \frac{4\mu[1+\rho(S-1)]}{rK}}\right\}. \tag{5}$$

Note that in the deterministic LV process all species survive with abundance $\tilde{x}$ as long as $\rho \leq 1$ with $\mu > 0$ [28]. Conversely, in the stochastic competitive environment the numbers of individuals of each species fluctuate, occasionally reaching extinction. Thus, the number of (co-)existing species S^* is a stochastic variable as well, and may be smaller than the overall number species S in the immigration flux from the larger basin, with $S^* \leq S$. The richness, denoted as $\langle S^*\rangle$, is defined as the average number of the (co-)existing species, and is related to the SAD via

$$\langle S^*\rangle = S(1 - P(0)) \tag{6}$$

which, intuitively, is determined by the probability that a species is present in the system, $1 - P(0)$.

No exact analytical solution for the high-dimensional master equation (2) is known for a general competition strength ρ. To understand the principles of the community organization and the impact of competition, immigration and demographic noise, we developed approximate analytical solutions to the master equation verified by Gillespie simulations (see SM for details).

III. RESULTS

A. Mean-Field Approximation

The full master equation (2) can be reduced to a one dimensional approximation for the marginal distribution $P(n)$ with effective birth-death rates (see SM). The SAD, $P(n)$, is obtained as a self-consistent stationary solution of this equation as

$$P(n) \equiv P_i(n_i = n)$$

$$= P(0)\frac{(r^+)^n(\mu/r^+)_n}{n!\prod_{n_i=1}^{n}\left(r^- + rn_i/K + r\rho\sum_{j\neq i}^{S}\langle n_j|n_i\rangle/K\right)}. \tag{7}$$

To obtain an analytical approximation to $P(n)$ we use a mean field closure for the unknown conditional averages $\langle n_j|n_i\rangle$ as $\left\langle\sum_{j\neq i}n_j|n_i\right\rangle \approx (S-1)\langle n\rangle$. Thus, (7) becomes a closed-form implicit equation for the probability distribution $P(n)$ which can be solved numerically. We have found a good agreement between exact stochastic simulation results and this mean-field approximation for most of the parameter space examined (see SM).

Following (6), the average richness in the mean-field approximation is (See SM)

$$\langle S^*\rangle = S\left(1 - \frac{1}{{}_1F_1[a,b+1;c]}\right), \tag{8}$$

where $P(0) = 1/{}_1F_1[a,b+1+1;c]$ is the normalization constant of $P(n)$ where ${}_1F_1[a,b;c]$ is the hypergeometric Kummer confluent function, with $a = \mu/r^+$, $b = [r^-K + r\rho(S-1)\langle n\rangle]/r$, and $c = r^+K/r$.

B. The system exhibits rich behavior with distinct regimes of population structures controlled by competition strength, immigration rate and the species number

Depending on the values of the competitive strength and the immigration rate, the number of species and the system size, the population can exhibit a number of different regimes of behavior, which can be categorized by their richness and the shape of their SAD, as visualized in Fig. 2 and described below. .

1. Richness regimes

In the classical deterministic LV model, the systems exhibits either an interior fixed-point with full coexistence of all species at abundances given by Eq. 5, or mass extinction with a single surviving species, in agreement with the well-known Gause's law of deterministic competitive exclusion [28]. By contrast, the stochastic model may also exhibit partial coexistence due to the abundance

fluctuations arising from the demographic noise whereby a subset of the species are driven to temporary extinction. Overall, the number of co-existing species and their abundances are determined by the balance between the immigration and stochastic competitive exclusion events. Three distinct richness regimes can be discerned as shown in Fig. 2, based on the variations of the richness of the system $\langle S^* \rangle$ in different regimes in the (ρ, μ, S) parameter space.

At low competition strength - region (a) in Fig. 2A - all species co-exist so that the richness of the system is equal to the number of species, same as in the deterministic regime $\langle S^* \rangle \approx S$. In this regime, each species effectively inhabits its own niche because the inter-species competition is not sufficiently strong to drive any of the species to extinction even in the presence of abundance fluctuations arising from the demographic noise. The probability for a species to be present is determined by the balance of its immigration rate and the death rate. At higher immigration rates this regime extends into regions with higher competition strength ρ: high immigration rates stabilize full richness populations even with a relatively high competition strength.

In the second regime - region (b) in Fig. 2A - only a fraction of the species are simultaneously present on average, which we denote as the partial coexistence regime. In this regime, the immigration influx is not high enough to prevent temporary stochastic extinctions of some species resulting from the competition.

At the very high competition strengths a complete exclusion regime - region (c) in Fig. 2A - is found. High competition along with the very low immigration rates act in unison such that the richness is less than two species. Although regime (c) may appear similar to regime (b) since both present partial coexistence, they are distinguished by key behavioral features as explained below.

Note that the stochasticity is central to the effect of the competition on the observed richness. Stochastic fluctuations increase the risk of extinction with increasing competitive overlap, unlike in the deterministic case where the richness is independent of the interaction strength for $\rho < 1$ [28].

2. SAD shape and modality regimes

Besides the richness, the balance between immigration and stochastic competitive extinctions also dictates the mean abundances of individual species and the species abundance distribution (SAD). When the immigration influx of individuals into the system is higher than the average out-flux due to the transient extinctions, shown in Fig. 2B as region (I), most species are forced away from extinction. In this regime, the SAD is unimodal with a peak at relatively high species abundances $\tilde{n}$ which is

approximately located at

$$\tilde{n} = \frac{K - \rho(S-1)\langle n \rangle}{2} \left\{ 1 \pm \sqrt{1 + 4\frac{(\mu - r^+)K}{r(K - \rho(S-1)\langle n \rangle)^2}} \right\},$$

$$(9)$$

which agrees with the simulation results, see Fig. 3; see SM.

At lower immigration rates - regime (II) in Fig. 2B - the immigration rate is insufficiently strong to overcome the competition driven temporary extinctions of some of the species, and the SAD develops an additional peak around $n = 0$ corresponding to the temporarily extinct species. The subset of the 'quasi-stably' co-existing species whose abundances fluctuate around $\tilde{n}$ within the high 'niche-like' abundance peak dominate the population number, punctuated by rare fluctuation-driven extinctions and the occasional invasion of a temporarily extinct species into the dominant population. By contrast, the dynamics of species in the $n = 0$ zero peak is characterized by the rapid turnover of the remaining species close to extinction.

At low immigration rates, the peak at (9) coincides with the deterministic stable solution in (5) (see SM)

$$\lim_{\mu \to 0} \tilde{n} = \lim_{\mu \to 0} \tilde{x}(\langle S^* \rangle) = \frac{K}{1 + \rho(\langle S^* \rangle - 1)}. \quad (10)$$

Namely, in the bimodal regime the coexisting dominant species are fluctuating around $\tilde{n}$ which, at low immigration, is the deterministic fixed point with $\langle S^* \rangle$ species. Thus, the dynamics of abundant species around the $\tilde{n}$ can be heuristically understood as spatially dependent diffusion in an effective potential well of the Fokker-Plank Equation (See Sec.II and SM).

Somewhat unexpectedly, at low immigration rate $\mu \lesssim .05$, the bimodal regime extends onto the neutral line at $\rho = 1$ where the SAD has been commonly believed to have the monotonically decreasing 'rare biosphere' shape [30, 70]. However, in this regime the competition is so strong that most of the time either no species are present at high abundance, or only one species survives in a kinetically 'frozen' long lived quasi-stable state with the abundance $\tilde{n} \simeq K$, as observed previously [72].

Furthermore, at the intermediate immigration rates and relatively high competition strengths we observe a unimodal behaviour with a peak at zero rather than at finite $\tilde{n}$ - region (III) in Fig. 2B. In this regime, the competition is strong enough so that the fluctuations competitively drive populations to temporary extinction before any species is able to establish a 'quasi-stable' state at a high abundance. All species undergo rapid turnover around zero resulting from the balance between random immigration and extinction events. This regime corresponds to what was previously described as the 'rare biosphere': fewer number of species are found at higher abundances resulting in a monotonically decreasing SAD. This SAD shape is classically recognized as a hallmark of a 'neutral-like' regime. However, as shown in Figure 2
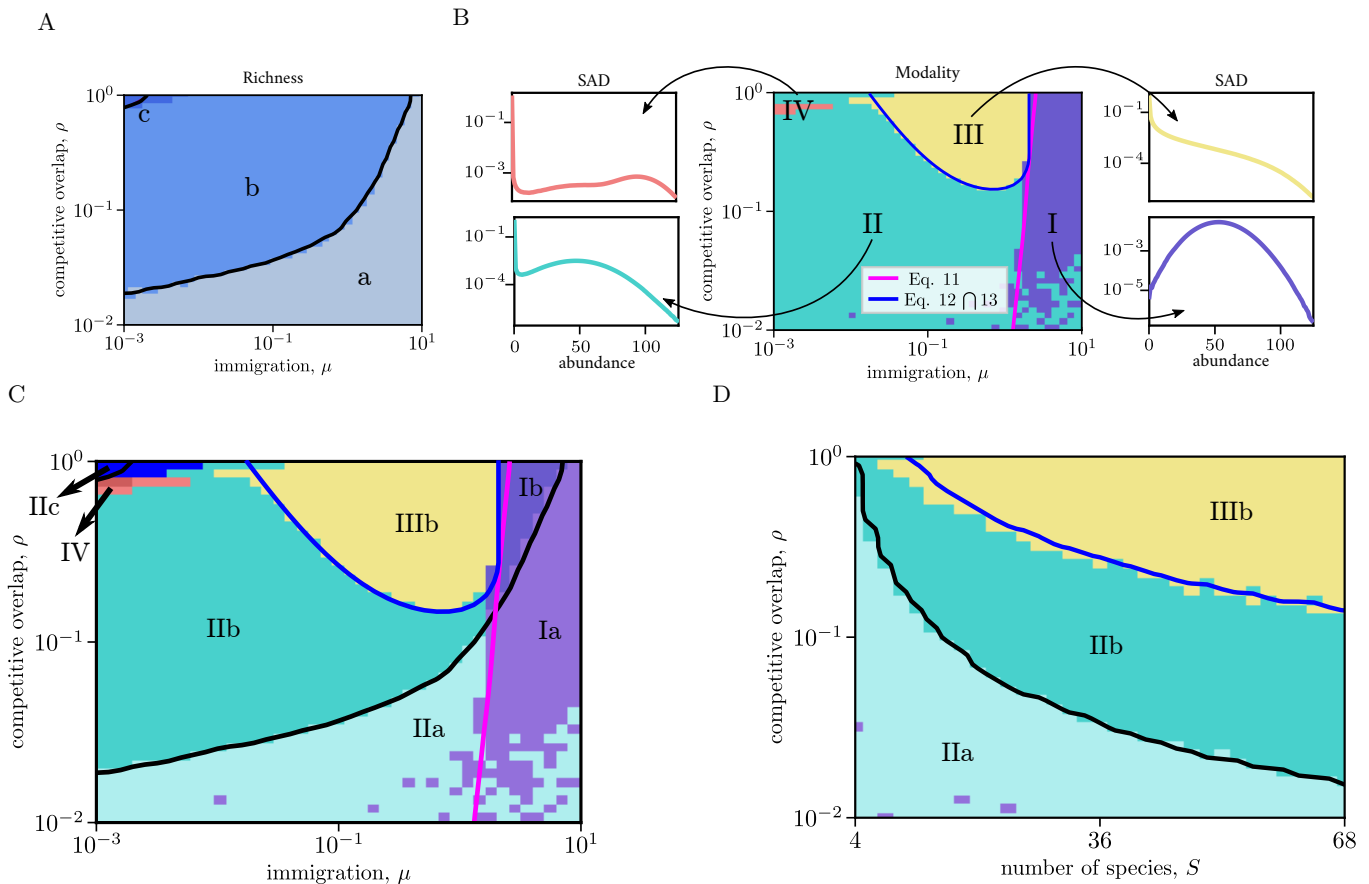
FIG. 2. Phenomenology of the population structures. Panel **A**: The system possesses three distinct richness phases. (a): full coexistence of all the species $\langle S^* \rangle \approx S$; (b): partial coexistence with $\langle S^* \rangle < S$; (c): a single species exists on average. Panel **B**: Different population regimes are distinguished by different SAD modalities. (I): immigration dominated regime with unimodal SAD at a typical abundance given by the positive root of $\tilde{n}$; (II): bimodal regime with species at non-zero abundance $\tilde{n}$ and a rapid species turnover peak a zero abundance; (III): 'rare biosphere' regime of a unimodal SAD with peak at zero abundance resulting from the rapid turnover of the temporarily extinct species; (IV) multimodal regime. Panels **C** and **D**: Intersection of the modality and richness regimes in the (μ, ρ) plane (**C**) and (S, ρ) plane (**D**); see text for discussion. In panels **A**, **B** and **C** the number of species $S = 30$. In panel **D** the immigration rate is $\mu = 10^{-1}$. For all panels; Colored regions represent data from simulation (see Methods), whereas boundaries from the mean-field approximation are represented by solid black lines. The solution for the master equation (2) is simulated using the Gillespie algorithm with $6 \cdot 10^8$ time steps, $r^+ = 2$, $r^- = 1$, and $K = 100$.

the unimodal regime (III) unexpectedly extends substantially beyond the neutral manifold $\rho = 1$, into the non-neutral regions with $\rho < 1$, and the monotonic-decreasing SAD persists even for competitions strengths as low as $\rho \approx 0.1$ - an order of magnitude weaker than the classical neutral regime. This challenges the common perception that the SAD of the 'rare biosphere' is necessarily closely related to neutrality.

Finally, we have found an entirely novel multimodal regime with more than two peaks - regime (IV) in Fig. 2 - which possesses one rapid turnover peak around extinction and multiple peaks at non-zero abundances. Similar to region (IIc), the peak at $n = 0$ comprises species which rapidly turnover around extinction. However, in addition to the peak at positive abundances K formed by one surviving species $(S^* = 1)$ in a meta-stable frozen state, this regime possesses a second peak at $\sim K/(1 + \rho)$ with two

simultaneously surviving quasi-stable species $(S^* = 2)$, following (10). The slow fluctuations between the states with $S^* = 1$ and $S^* = 2$ result in the appearance of the SAD with two non-zero modes at quasi-stable dominance abundance, $\tilde{n} \sim K$ and $\tilde{n} \sim K/(1 + \rho)$ observed in the region (IV); these two peaks are only visibly separated when the richness is low and carrying capacity is high, as follows from (10).

The transitions between the different regimes and the corresponding changes in the SAD shapes are illustrated in Fig. 3. Generally, at low competition strength ρ, where the species are practically independent of each other and reside in largely non-overlapping niches, their typical abundance $\tilde{n}$ is close to the carrying capacity K. Increasing competition strength ρ makes it harder to sustain co-existing species at high abundances, and accordingly $\tilde{n}$ decreases, as illustrated in the top pan-

els of Fig. 3A) and Fig. 3B). With further increase in ρ the system behavior bifurcates depending on the immigration rats μ. At high immigration rates, $\mu \gtrsim 0.05$, the competition-driven decrease in $\tilde{n}$ continues up to the critical competition strength (calculated in the next section) where the peak around $\tilde{n}$ disappears (top right panel of Fig. 3A) and Fig. 3B), as the system is not able to sustain 'quasi-stable' niche-like species co-existence. This corresponds to the transition from bimodal region (II) to the 'rare biosphere' neutral-like region (III) in Fig. 2). At lower immigration rates (top left panel of Fig. 3A) and Fig. 3B)), further increases in the competition strength eventually cause mass species extinctions which allows the remaining few dominant species to maintain higher abundances (region (III) Fig. 2). As $\rho \to 1$, the system transitions to the region (IIc) of the Fig. 2: only one dominant species remains, as described in [72], with abundance K.

3. Global Phase Diagram and Regime Boundaries

In this section we describe the complete phase diagram of the system defined by the intersection of the different richness and the SAD shape/modality regimes, derive the regime boundaries and discuss the transitions between them, as shown in the (μ, ρ) space in Fig. 2C, and in (S, ρ) space in Fig. 2D. We show that the boundaries between different regimes observed in simulations can be understood within simple mean field theories, and discuss the underlying physical factors responsible for the transitions between different regimes.

We define the boundary between the full coexistence (a) and partial coexistence (b) regimes to be at $\langle S^* \rangle = S - 1/2$: the midpoint between full richness $S^* = S$ and the loss of 1 species on average. Similarly, the boundary between the partial coexistence (b) and exclusion (c) regimes is located at $\langle S^* \rangle = 3/2$, that is to say where the richness is between one and two species such that on average only 1 species is present in regime (c).

To derive the boundaries corresponding to the transitions of the SAD modality regimes, we use discrete derivatives of the approximated SAD to determine the existence of peaks and their location (See SM). The immigration dominated regime (I) is characterized by a unimodal SAD with a peak at the positive root of $\tilde{n}$ given in (9). Compared to this immigration dominated regime, the neighboring bimodal and monotonically-decreasing unimodal regimes - regions (II) and (III) respectively - differ by the emergence of a new mode at zero abundance.

Thus, the boundary that defines transitions to either regime (II) or (III) from the immigration dominated regime (I) is described by a flattening of SAD at $n = 0$: $\partial P(n)/\partial n|_{n=0} = 0$ which, in the discrete case, heuristically corresponds to $P(0) = P(1)$. Combining this condition for the boundary with the global-balance of the master equation (2) results in the rate balance equation, $\langle q_i^+(\vec{n})|n_i = 0 \rangle = \langle q_i^-(\vec{n})|n_i = 1 \rangle$.
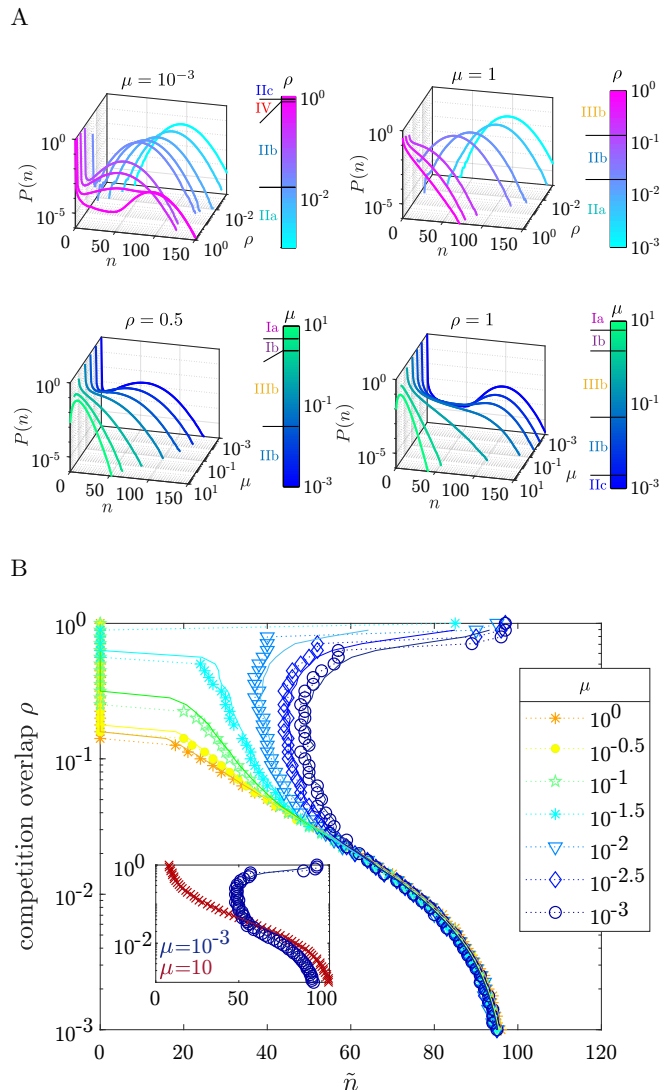

FIG. 3. SAD changes between different regimes. Panel **A**: (upper left) Simulation results for species abundance distributions (SADs) for fixed $\mu = 10^{-3}$ as a function of ρ. (upper right) same for $\mu = 1$. Different values of the interaction strength ρ are emphasized with different colors indicated in the color-bar. (lower left) Simulation results for SADs as a function of μ for fixed $\rho = 0.5$ (lower right) same for $\rho = 1$. Different immigration rates μ are emphasised with different color shown in the color-bar. **B**: The non-zero mode of the SAD given by the positive solution of $\tilde{n}$ representing the dominant species abundance as a function of ρ for different values of μ. Markers and dotted lines represent simulation results, while solid lines are given from analytic analysis, (9).

In the mean-field approximation, this boundary is found at

$$\mu = r^- + \frac{r}{K}[1 + \rho(S - 1)\langle n \rangle]. \tag{11}$$

This equation recovers the similar transition for $\rho = 1$ derived independently in [72].

The boundary between the bimodal regime (II) and

the 'rare biosphere' regime (III) is characterized by the disappearance of the peak at high abundance $\tilde{n}$ in (9). In the bimodal regime at least one solution to $\tilde{n}$ is real and positive, then a maximal, real peak-location exists. Conversely, in the 'rare biosphere' regime, both solutions of $\tilde{n}$ are negative or imaginary. We find that the boundary between the real and imaginary $\tilde{n}$ is

$$r(K - \rho(S-1)\langle n \rangle)^2 = 4(r^+ - \mu)K \qquad (12)$$

and the transition line between positive and negative solutions, $\tilde{n} = 0$, is

$$\frac{(K - \rho(S-1)\langle n \rangle)^4}{16} = 1 + \frac{K(\mu - r^+)}{r}. \qquad (13)$$

The intersection of these two conditions defines the 'rare biosphere' regime and is shown as the blue line in Fig. 2B,C.

The modality and the richness of the system are also affected by the number of species S as shown in Fig. 2D. In brief, the frequency of the immigration events rises as more species are present in the immigration flux. Increased immigration causes the total population to rise without providing more room for each species in the system; this increases the stochastic competition, driving more species to extinction. Hence, as S increases, the transition from the bimodal regime (II) to the unimodal regime (III) occurs at lower values of competition strength ρ, and the fraction of the concurrently surviving species decreases. This effect has been qualitatively observed experimentally [80], and we return to it in the Discussion.

These analytical expressions for the regime boundaries - confirmed by stochastic simulations - provide insights into the effects of different control parameters on the regime boundaries. In particular, using the low μ deterministic approximation for $\langle n \rangle \approx K/[1 + \rho(S-1)]$, shows that the location of the boundary of the 'rare biosphere' regime grows proportionally to the carrying capacity and is a decreasing function of the number of species S. Thus, the size of the 'rare biopshere' neutral-like regime increases with the number of species S as shown in Fig. 3D, whereas increasing the carrying capacity shrinks this regime (See SM).

C.   Kinetics of the species turnover, extinction and recovery underlie the transitions between different regimes

So far we have focused on the steady-state properties of the system, such as the dominant species abundance, SAD modality, and richness to categorize the different regimes. However, the transitions between different regimes are closely related to the underlying kinetics of species turnover and fluctuations, which are investigated in this section.

The kinetics of an individual species change drastically between the unimodal 'rare biosphere' regime (III)

and the regimes that exhibit a peak in SAD at non-zero abundance as shown in Fig. 4A that contrasts the kinetics in these cases. In regime (III), all species undergoes rapid turnover in the relatively broad range of abundances around extinction. In contrast, in the 'niche-like' regimes (I, II, and IV) the 'quasi-stable' dominant species undergo fast fluctuations around the co-existence peak at $\tilde{n}$ in addition to fast turnover of the remaining species near extinction. The 'niche-like' regimes also possess slow timescales corresponding to individual species leaving the high abundance peak as they are temporarily driven towards extinction, and the reverse invasions of temporarily extinct species into the dominant 'niche-like' peak.

To characterize the differences in the kinetics in different regimes, we calculate the mean first-passage times (MFPT) of the transitions between different abundance levels characterizing different regimes, denoting the MFPT for a species transition from an abundance a to another abundance b as $T(a \rightarrow b)$. Similarly, $T(a \rightarrow a)$ refers to the mean time of return to an abundance a having left that same abundance. The MFPT is calculated from the one-dimensional backward Master equation (see SM).

Although these times are important indicators of the system dynamics, the MFPT ratios of two processes/events is more informative than the MFPT of each event separately; this ratio measures the discrepancy between the timescales at which these events occur.

To understand the intrinsic kinetics that give rise to the different regimes in Fig. 2, we first focus on the ratio of the MFPTs of the transitions from dominance to exclusion over the mean time of return to the dominant abundance level (starting from the dominant abundance level), $T(\tilde{x}(\langle S^* \rangle) \rightarrow 0)/T(\tilde{x}(\langle S^* \rangle) \rightarrow \tilde{x}(\langle S^* \rangle))$, shown in (Fig. 4B). Recall that $\tilde{x}$ is the solution given in (5); this deterministic solution is a natural extension of the peak $\tilde{n}$ in regimes where positive modes are non-existent. As explained below, this ratio underlies the changes in the modality of the SAD as a function of the immigration rates and the competition strength.

Large values of the ratio $T(\tilde{x}(\langle S^* \rangle) \rightarrow 0)/T(\tilde{x}(\langle S^* \rangle) \rightarrow \tilde{x}(\langle S^* \rangle))$ imply that the extinction rate from $\tilde{x}(\langle S^* \rangle)$ is much slower than the rate of local fluctuations in the effective potential well around $\tilde{x}(\langle S^* \rangle)$. Accordingly, Fig. 4B shows that this ratio is high in the bimodal and immigration-dominated regimes. Conversely, this ratio is lower within the 'rare biosphere' regime that does not possess a high abundance peak with 'quasi-stable' co-existing species. This ratio approximately delineates the 'rare biosphere' neutral-like regime from the 'niche-like' regimes, as shown in Fig. 4B: the contour lines qualitatively recover the boundaries of region IIIb in Fig. 2C.

The second ratio, which underlies the richness transitions in the system, $T(0 \rightarrow \tilde{x}(\langle S^* \rangle))/T(0 \rightarrow 0)$ (Figure. 4 panel C) relates the mean return time to extinction to the invasion time from extinction at zero abundance to dominance at $\tilde{x}$. High values of this ratio indicate that, for

an extinct species, the mean invasion times are longer than return times back to extinction. This MFPT ratio approximates the ratio of the average number of temporarily extinct species, $S - \langle S^* \rangle$ to the average number of existing species, $\langle S^* \rangle$, see Fig. 4C. Consequently, the ratio quantitatively recovers the boundaries of richness regimes in Fig. 2 in most regions of the parameter space. These MFPT ratios can be understood as the reciprocal of the rates ratios which describe how much more frequently an event occurs than the other. Further discussion on the dynamical features are presented in the SM.

Overall, the 'niche-like' Regimes I, II and IV are characterized by a relatively stable behavior; generally species stay longer about the dominant species abundances,punctuated by the occasional crossings between dominance to nearly-extinct states and the reverse invasions from extinction into the dominance. The transition between partial coexistence (b) to regime of competitive exclusion (c) is captured by the non-monotonic behaviour of the ratio as shown in Fig. 4C. Surprisingly, unlike the other regimes, increasing the competition strength in the competitive exclusion regime (c) increases the stability of the dominant species abundance: return times to the dominant abundance are much shorter than the time to extinction for the single species in the frozen 'quasi-stable' state. Conversely, the 'rare biosphere' regime (III) features rapid dynamics where species cycle rapidly between extinction and a broad range of abundances without establishing 'quasi-stable' states with slow turnover. These different dynamic types are illustrated by illustrative trajectory plots in Fig. 4A.

D. The abundances of different species are weakly anti-correlated

So far, we have investigated the single species marginal abundance distribution $P(n)$ and the average richness $\langle S^* \rangle$. However, the species are not independent of each other due to the inter-species competitive interactions. It has been suggested that inter-species correlations reflect on the underlying community structure and the phase space [81, 82].To investigate the connection between the population structure and the cross-species correlations, we calculated the cross-species abundances correlations, quantified via the Pearson correlation coefficient, as shown in Fig. 5A. The population exhibits weak cross-species anti-correlation that increases with the competition strength ρ. This is expected given that the death rate of each species increases with the abundance of the other species and, consequently, these cross-species influences are more pronounced at high competition strengths. Conversely, higher immigration rates ensure that the abundance fluctuations of different species are less likely to be correlated with those of other species. Thus, the anti-correlation is most pronounced in the high competition and low immigration regime.

Furthermore, the impact of individual species on the total population size varies between community structures, which can be quantified by the correlation between the total population size J and individual abundances. We found that the individual species abundances are positively correlated with the total abundance $J = \sum_i n_i$, which also fluctuates as the individuals of all species undergo birth and death events. Interestingly, as shown in Fig. 5B, the magnitude of this correlation $\mathrm{cov}(J, n_i)/\sigma_n \sigma_J$ exhibits inverse trends compared to the inter-species anti-correlation: the correlation $\mathrm{cov}(J, n_i)/\sigma_n \sigma_J$ is weaker when the cross-species anti-correlation is stronger. The magnitude of the correlation between the total population size J and a species abundance n exhibits similar behavior to the average richness: $\mathrm{cov}(J, n_i)/\sigma_n \sigma_J$ is high in the high immigration, low competitive overlap regime and is low otherwise. This behaviour may be understood heuristically: whereas each species in a system with S^* dominant species only contributes $\sim J/S^*$ to the total population size.

Somewhat unexpectedly, neither the inter-species correlations nor the correlations between the species abundance and the total abundance distinguish between the different modality regimes but rather both increase with the richness. As expected, our mean-field approximation works best at very low $\mathrm{cov}(n_i, n_j)/\sigma_{n_i} \sigma_{n_j}$, whereas our mean-field deviates from the solution at anti-correlation gets stronger (see SM).

IV. SUMMARY AND DISCUSSION

Ecological systems display a wide variety of different behavior regimes that have been commonly analysed through a limited number of paradigmatic models such as the 'niche' and 'neutral' theories. However, it remains incompletely understood what features of ecological population structure and dynamics are universal and which are system specific, how different models relate to each other, and what behavior is expected in the full range of the parameter space. Using a minimal model of the competitive population dynamics with demographic noise, we have investigated the different regimes of the population structures and dynamics as a function of the immigration rate μ, competitive overlap ρ, and the number of species S. Although this minimal model may not fully capture the more complex interaction structures of many ecological communities, it already exhibiting rich and unexpected behaviours paralleling many experimentally observed ones (see Table I below and Table S1 in SM), and illuminates the underlying mechanisms that shape population structures in different ecosystems.

We have focused on the system richness reflecting the number of the co-existing species, and the SAD shape as the characteristics of the different population regimes, using a combination of simulations and analytical mean-field approaches. Our analysis shows that the ecosystem behaviors can be partitioned into different regimes
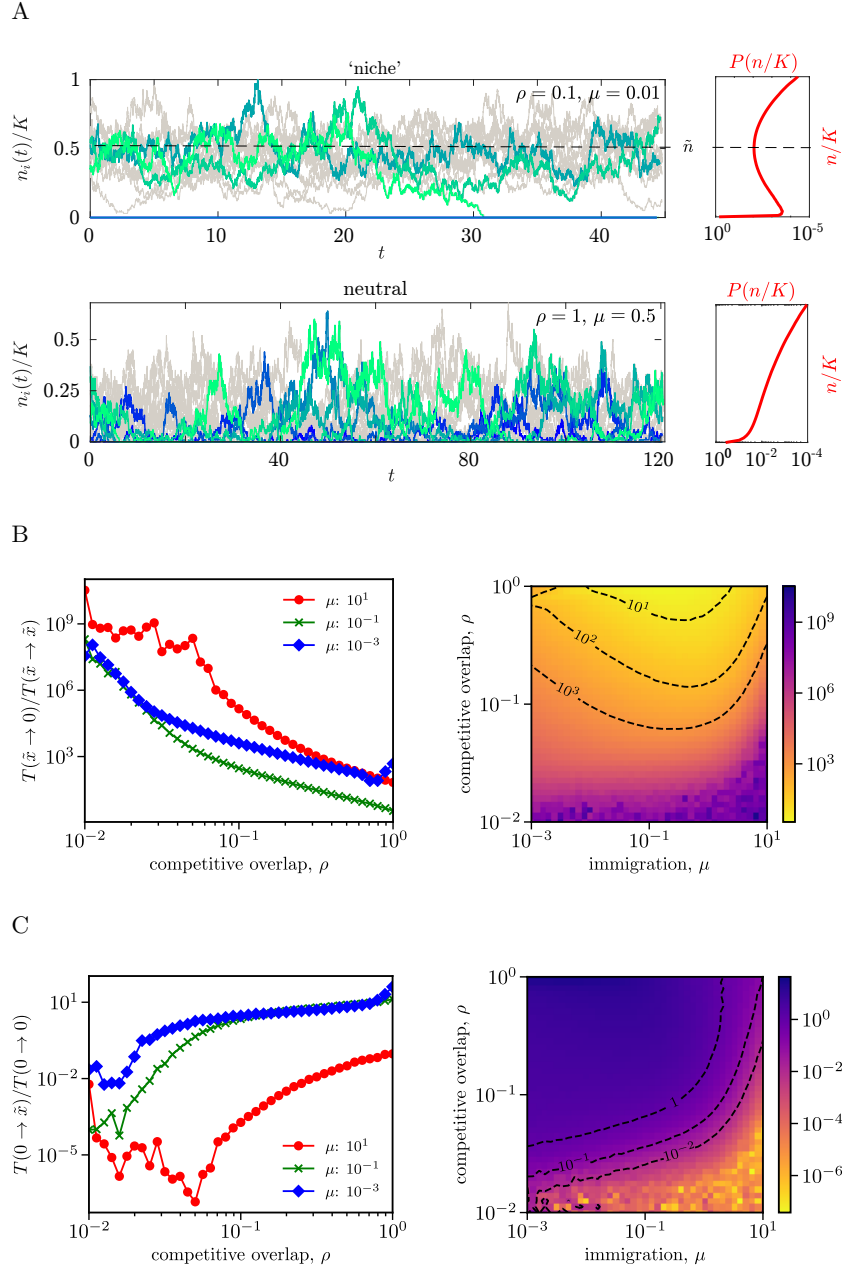
A

B

C

FIG. 4. Kinetics of species extinction, invasion and turnover. Panel **A**: Sample of the trajectories of the species abundances (grey lines). We highlight five species' trajectories for visibility. (Upper panel): stable 'niche-like' dynamics, where the abundances of the dominant species mostly fluctuate in the vicinity of $\tilde{n}$, with occasional transitions from the dominance to nearly-extinct states. The red curve represents the corresponding bimodal SAD. Lower panel shows the erratic dynamics obtained in the 'rare biosphere' regime, where all species are rapidly fluctuating close to extinction. The SAD in this case is unimodal monotonically decreasing function. Panel **B**: The MFPT ratio $T(\tilde{x} \to 0)/T(\tilde{x} \to \tilde{x})$ as a function of ρ (left). For very weak immigration rates $\mu \approx 10^{-3}$ the ratio is non-monotonic in competition strength, revealing regime (c) in Fig. 2. The MFPT ratios as a function of both μ and ρ is represented with a color-map (right). **C**: The MFPT ratio $T(0 \to \tilde{x})/T(0 \to 0)$ as a function of the competition overlap (left) and as a function of both ρ and μ (right). This ratio qualitatively captures the richness behaviour in Fig. 2. Both panels (B) and (C): the values are represented with the logarithmic color scale.

of richness and SAD shape/modality, parameterized by the immigration rate and the competitive overlap.

Our model recovers the expected limits of the well known 'neutral-like' and the 'niche-like' regimes. In particular, at $\rho = 1$ and intermediate values of μ, the

SAD has the 'rare-biosphere' monotonously decreasing shape characteristic of the classical neutral regime. On the other hand, at low competition strength, the system SAD exhibits a peak at high species abundance where all species co-exist, effectively occupying distinct ecological

A

$$\mathrm{cov}(n_i, n_j)/\sigma_{n_i}\sigma_{n_j}$$

B

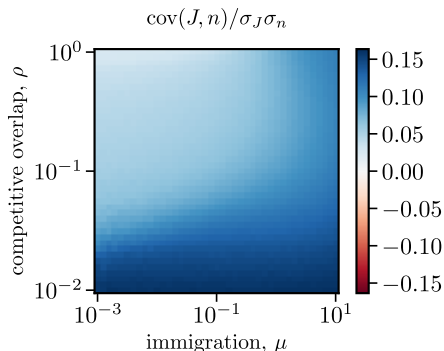$$\mathrm{cov}(J, n)/\sigma_J\sigma_n$$
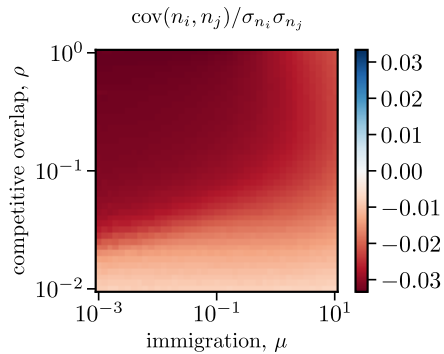
FIG. 5. Abundance correlations. Panel **A**: Pearson correlation coefficient between the abundances of any two different species. Panel **B**: Pearson correlation coefficient between the total population size $J = \sum n_j$ and an abundance of any species. Correlations were calculated from Gillespie simulation time course data with $6 \cdot 10^8$ time steps.

niches.

Note that even independent species with no inter-species competition with $\rho = 0$ may present either a uni-modal or bimodal SAD depending on the immigration rate, see Fig. 2B&C. Unlike the immigration dominated high abundance peak at high immigration rates, at the very low immigration rates the SAD is peaked around zero due to high extinction probability solely from the intra-species competition.

Changes in the SAD between different regimes, reflected in the changes in the locations and the heights of the SAD peaks as a function of the immigration and the competition strength, occur through different routes. For instance, starting at the bimodal regime (II) at $\rho = 1$, as the immigration rate increases, the SAD peak height gradually decreases without changing significantly its location, until it finally disappears at the boundary of the 'rare biosphere' regime (III). By contrast, at lower competition strengths $\rho < 1$, the transition from the bi-modality to the 'rare biosphere' regime occurs via simultaneous changes in the peak's height and location. This is discussed in Sec. IIIB.

We found that for the intermediate immigration

rates the system maintains the monotonically decaying 'neutral-like' SAD in regime (III) even at rather low competition strength ($\rho \approx 0.1$) contrary to the common expectation that different species inhabit separate niches away from neutrality. Conversely, at low immigration rates, the system SAD unexpectedly maintains the peak at non-zero abundance characteristic of 'niche-like' regimes even for the high values of the competition strength ρ usually considered to be in the 'neutral-like' domain (regime (IIc)); see Sec. IIIB and Figure 2.

We have also uncovered an unusual - and to the best of our knowledge hitherto not described - regime characterized by the multi-modal SAD with more than one positive, 'quasi-stable' abundance peak (Regime (IV) in Fig 2). This multi-modality arises from the richness fluctuations in this regime: the number of co-existing species is switching randomly between two relatively long-lasting states with $S^* = 1$ and $S^* = 2$. Thus, one peak of the SAD is found around $\sim K$ and the other one in the vicinity of $\sim K/2$, as explained in Sec. IIIB. We observe that for low K, the multimodal regime is non-existent and appears as K increases; see the corresponding phase diagrams in SM.

We show that the population structures in different regimes stem from the underlying dynamics of species fluctuations, extinctions and invasions. In the 'rare biosphere' neutral-like regimes, all species undergo relatively fast turnover around extinction. This is reflected in the low ratio of the turnover to the extinction mean first-passage times. Conversely, in the 'niche-like' regimes the system develops two additional time scales: relatively fast fluctuations about the high abundance peak, and the long waiting times for the transitions from the 'quasi-stable' co-existence at high abundance to extinction. Accordingly, the ratio of the mean extinction time to the mean time of return to dominance is higher in the 'niche-like' regime, as discussed in Sec. IIIC.

Interestingly, ecological regimes akin to those predicted by our demographic noise model (except for the multimodal SAD regime) have been also found using deterministic, noiseless LV models with a random matrix of inter-species competitive interaction strengths [61, 78, 80, 83, 84]. However, the underlying mechanisms that give rise to the apparently similar regimes in the two model types are very different. In the demographic noise model, the partial richness 'niche-like' regime is formed by the coexistence of some species at a positive abundance and temporary extinctions of other species induced by the stochastic abundance fluctuations. By contrast, in the deterministic LV models with random asymmetric interactions, this regime is formed from a large number of fixed points where different sets of species are deterministically excluded. At higher interaction strengths, the system transitions to the deterministically chaotic behavior that resembles the 'neutral-like' regimes, however the nature of the species turnover and the SAD shape are very different to the behaviour we described above [61, 80, 85].

The existence of the predicted regimes and the transitions between them can be tested experimentally by measuring the SAD and the dynamics of the species abundances in ecosystems with varying immigration and competition strengths. Long-term observations may provide measurements of the stationary species abundance distributions [86] although the steady-state SAD may be difficult to estimate due to the limited amount of data. It may be difficult to experimentally determine and control the immigration rate, the competition strength, and carrying capacity, but practically useful proxies for these parameters exist. For example, the flow rate carrying bacteria into a chamber of a microfluidic device is a well controlled quantity that approximates well the immigration rate for populations encased in the chamber [**?**]. Furthermore, measurements of the SADs and the community compositions have become more attainable due to the advances in single cell gene sequencing techniques [1, 12, 80]. Another commonly used and robustly estimated experimental observable is the species rank abundance (SRA), which can be used to infer the SAD to which it is closely mathematically related, although in practice the conversion might be constrained by limitations of noise and quantity of the experimental data.

Despite these difficulties, the asymptotic behaviour of the SADs may provide indication of qualitative dissimilarities between the various regimes to discern different regimes of behavior among the experimental observations. In the mean-field approximation in our model the asymptotic behaviour of the SAD on the neutral line $\rho = 1$ approximates a power law with an exponential cutoff (see SM) - similar to the commonly used neutral birth-death models with the fixed total population size [70, 71]. Notably, the Yule process that is often used to model neutral processes also results in the SAD of a similar form. However, the Yule process is substantially different from the model of this paper because it does not include inter-species interactions and reaches the steady state SAD only if $r^+ < r^-$.

In Table 1, we qualitatively compare the family of the regimes predicted by our model to the various behaviors inferred from experimental findings based on the SAD measurements and population abundance time series. The notable abundance of the neutral ecosystems observed experimentally may pertain to our finding (Section IIIB) that the 'neutral-like' 'rare biosphere' regime extends substantially beyond the neutral line $\rho = 1$: non-neutral communities appear neutral as they exhibit SAD's characteristic of neutral communities, such as gastrointestinal microbiomes [87]. Furthermore, multimodal SAD's predicted by our model that are related to the richness fluctuations may provide an explanation for the multimodal SADs observed in some ecological data, complementary to the current explanations such as spatial heterogeneity or emergent neutrality [60, 88]

One quantity that is experimentally relatively easy to control is the total number of species S. The regimes predicted by the model and the transitions between them

System (Ref.)	Regimes
microbial competition[80]	stable full coexistence (IIa)
	stable partial coexistence (IIb)
	persistent fluctuation (IIIb)
global birds species [89]	unimodal - log skew (I)
plankton [90]	power-law decay (III)
coral [88]	multimodal (IV)
arthropods [91]	multimodal (IV)
T-cell receptors [92]	bimodal (II)
	unimodal (III)
microbial competition [93]	'neutral-like' (III)
	'niche-like' (I & II)
gastrointestinal microbiomes [87]	'neutral-like' (III)

TABLE I. Qualitative classification of observed population regimes in various ecological systems.

shown in Fig. 2D show similarities with the experimentally observed ones - which were previously explained within the deterministic LV models with random interaction matrix [80]. As shown in Fig. 2D; our model yields 'neutral-like' regimes for high S and ρ, which are characterized by erratic dynamics, and 'niche-like' behavior with more stable behavior for either low S or ρ. This qualitatively agrees with observed phase-space the in [80], which for strong competition and large pool of species the system presents 'persistent fluctuation' regime, while for small species pool or weak competition exhibit 'stable full/partial coexistence'. The fact that both the deterministic LV model with random interaction matrix and the homogeneous LV model with demographic noise are in qualitative agreement with the experimental data raises interesting and important questions concerning the role of stochastic and deterministic dynamics on community composition.

Another quantity that may enable qualitative and quantitative testing of different models is the carrying capacity K which may be controllable experimentally in some systems. As shown in SM, 'rare biosphere' regime shrinks in size with increasing K because a higher carrying capacity sustains higher average abundance, and larger (less likely) fluctuations are needed for the extinction events to occur. Higher average abundance together with insufficiently strong fluctuations, result in longer MFPTs from dominance to extinction abundances and vice-versa. This might be captured by the dependence of K in (11), but further work on the mean-field approximations is needed. Unfortunately, rarer turnover events imply longer times to reach the steady state, thus comparing our analytical prediction of the dependence on very large K becomes unfeasible using simulations.

We expect that the minimal model of this paper can be used for more complicated scenarios, including incorporating speciation to probe the interaction of the natural selection, inter-species interactions and population diver-

sity and structure. Furthermore, the deterministic models inspire further extension of our framework to more complex distributions of the interaction network $\rho_{i,j}$. Finally, our examination of the local ecosystem within an island in the mainland-island model (see Fig. 1), can be expanded to a many-island model which allows studying differences in dynamics between the local community and metacommunity, a prominent topic for conservation ecologists and the study of the human microbiome, amongst others.

METHODS

The solution for the master equation (2) is simulated using the Gillespie algorithm with 10^8 time steps. We use $r^+ = 2$, $r^- = 1$, $K = 100$. Modalities' classification is numerically executed after smoothing the simulated SAD. The MFPT is evaluated via the simulated SAD ($\tilde{x}(S^*)$ is rounded), where a uni-dimensional approximation of the process is considered, see details in SM.

ACKNOWLEDGMENTS

[1] C. Ratzke, J. Barrere, and J. Gore, Strength of species interactions determines biodiversity and stability in microbial communities, Nature ecology & evolution **4**, 376 (2020).

[2] D. Tilman, Resource competition between plankton algae: an experimental and theoretical approach, Ecology **58**, 338 (1977).

[3] S. L. Strom, Microbial ecology of ocean biogeochemistry: a community perspective, science **320**, 1043 (2008).

[4] K. R. Foster, J. Schluter, K. Z. Coyte, and S. Rakoff-Nahoum, The evolution of the host microbiome as an ecosystem on a leash, Nature **548**, 43 (2017).

[5] K. Z. Coyte, J. Schluter, and K. R. Foster, The ecology of the microbiome: networks, competition, and stability, Science **350**, 663 (2015).

[6] F. A. Gorter, M. Manhart, and M. Ackermann, Understanding the evolution of interspecies interactions in microbial communities, Philosophical Transactions of the Royal Society B **375**, 20190256 (2020).

[7] L. M. Merlo, J. W. Pepper, B. J. Reid, and C. C. Maley, Cancer as an evolutionary and ecological process, Nature reviews cancer **6**, 924 (2006).

[8] I. Kareva, Cancer ecology: Niche construction, keystone species, ecological succession, and ergodic theory, Biological Theory **10**, 283 (2015).

[9] M. Smart, S. Goyal, and A. Zilman, Roles of phenotypic heterogeneity and microenvironment feedback in early tumor development, Physical Review E **103**, 032407 (2021).

[10] A. I. Tauber, The immune system and its ecology, Philosophy of science **75**, 224 (2008).

[11] P. Schmid-Hempel and D. Ebert, On the evolutionary ecology of specific immune defence, Trends in Ecology & Evolution **18**, 27 (2003).

[12] N. Shakiba, A. Fahmy, G. Jayakumaran, S. McGibbon, L. David, D. Trcka, J. Elbaz, M. C. Puri, A. Nagy, D. van der Kooy, *et al.*, Cell competition during reprogramming gives rise to dominant clones, Science **364** (2019).

[13] D. Tilman, *Resource competition and community structure* (Princeton university press, 1982).

[14] P. J. Morin, *Community ecology* (John Wiley & Sons, 2009).

[15] S. Tuljapurkar, *Population dynamics in variable environments*, Vol. 85 (Springer Science & Business Media, 2013).

[16] O. Budzinski, Monoculture versus diversity in competition economics, Cambridge Journal of Economics **32**, 295 (2007).

[17] Y. H. Koura, Y. Zhang, and H. Liu, Competitive interaction model for online social networks' users' data forwarding at a subnet, Mathematical Problems in Engineering **2017** (2017).

[18] R. Lewin, Finches show competition in ecology, Science **219**, 1411 (1983).

[19] D. Lack and L. David, *Darwin's finches* (CUP Archive, 1983).

[20] B. Grant and P. Grant, Darwin's finches: population variation and sympatric speciation, Proceedings of the National Academy of Sciences **76**, 2359 (1979).

[21] A. Pocheville, The ecological niche: history and recent controversies, in *Handbook of evolutionary thinking in the sciences* (Springer, 2015) pp. 547–586.

[22] D. Zuppinger-Dingley, B. Schmid, J. S. Petermann, V. Yadav, G. B. De Deyn, and D. F. Flynn, Selection for niche differentiation in plant communities increases biodiversity effects, Nature **515**, 108 (2014).

[23] J. Silvertown, Plant coexistence and the niche, Trends in Ecology & evolution **19**, 605 (2004).

[24] J. J. Cullen and J. G. MacIntyre, Behavior, physiology and the niche of depth-regulating phytoplankton, Nato Asi Series G Ecological Sciences **41**, 559 (1998).

[25] S. M. Melo-Merino, H. Reyes-Bonilla, and A. Lira-Noriega, Ecological niche models and species distribution models in marine environments: A literature review and spatial analysis of evidence, Ecological Modelling **415**, 108837 (2020).

[26] J. Aguirre-Gutiérrez, H. M. Serna-Chavez, A. R. Villalobos-Arambula, J. A. Perez de la Rosa, and N. Raes, Similar but not equivalent: ecological niche comparison across closely–related m exican white pines, Diversity and distributions **21**, 245 (2015).

[27] M. Badali and A. Zilman, Effects of niche overlap on coexistence, fixation and invasion in a population of two interacting species, Royal Society open science **7**, 192181 (2020).

[28] J. A. Capitán, S. Cuenda, and D. Alonso, How similar can co-occurring species be in the presence of competition and ecological drift?, Journal of the Royal Society Interface **12**, 20150604 (2015).

[29] G. Bell, Neutral macroecology, Science **293**, 2413 (2001).

[30] S. P. Hubbell, *The unified neutral theory of biodiversity and biogeography (MPB-32)*, Vol. 32 (Princeton University Press, 2001).

[31] J. Chave, Neutral theory and community ecology, Ecology letters **7**, 241 (2004).

[32] N. J. Gotelli and B. J. McGill, Null versus neutral models: what's the difference?, Ecography **29**, 793 (2006).

[33] R. A. Blythe, Neutral evolution: a null model for language dynamics, Advances in complex systems **15**, 1150015 (2012).

[34] J. P. Grover, J. Hudziak, and J. D. Grover, *Resource competition*, Vol. 19 (Springer Science & Business Media, 1997).

[35] M. Begon, C. R. Townsend, and J. L. Harper, *Ecology: from individuals to ecosystems*, Sirsi) i9781405111171 (2006).

[36] J. Adams, *Species richness: patterns in the diversity of life* (Springer, 2009).

[37] M. Kéry and J. A. Royle, *Applied Hierarchical Modeling in Ecology: Analysis of distribution, abundance and species richness in R and BUGS: Volume 2: Dynamic and Advanced Models* (Academic Press, 2020).

[38] A. Nias, Clone size analysis: a parameter in the study of cell population kinetics, Cell Proliferation **1**, 153 (1968).

[39] S. Rulands, F. Lescroart, S. Chabab, C. J. Hindley, N. Prior, M. K. Sznurkowska, M. Huch, A. Philpott, C. Blanpain, and B. D. Simons, Universality of clone dynamics during tissue development, Nature physics **14**, 469 (2018).

[40] P. C. de Greef, T. Oakes, B. Gerritsen, M. Ismail, J. M. Heather, R. Hermsen, B. Chain, and R. J. de Boer, The naive t-cell receptor repertoire has an extremely broad distribution of clone sizes, Elife **9**, e49900 (2020).

[41] B. J. McGill, R. S. Etienne, J. S. Gray, D. Alonso, M. J. Anderson, H. K. Benecha, M. Dornelas, B. J. Enquist, J. L. Green, F. He, *et al.*, Species abundance distributions: moving beyond single prediction theories to integration within an ecological framework, Ecology letters **10**, 995 (2007).

[42] T. J. Matthews and R. J. Whittaker, On the species abundance distribution in applied ecology and biodiversity management, Journal of Applied Ecology **52**, 443 (2015).

[43] C. Rahbek and G. R. Graves, Multiscale assessment of patterns of avian species richness, Proceedings of the National Academy of Sciences **98**, 4534 (2001).

[44] S.-H. Hong, J. Bunge, S.-O. Jeon, and S. S. Epstein, Predicting microbial species richness, Proceedings of the National Academy of Sciences **103**, 117 (2006).

[45] P. B. Adler, E. W. Seabloom, E. T. Borer, H. Hillebrand, Y. Hautier, A. Hector, W. S. Harpole, L. R. O'Halloran, J. B. Grace, T. M. Anderson, *et al.*, Productivity is a poor predictor of plant species richness, science **333**, 1750 (2011).

[46] E. Valencia, F. de Bello, T. Galland, P. B. Adler, J. Lepš, E. Anna, R. van Klink, C. P. Carmona, J. Danihelka, J. Dengler, *et al.*, Synchrony matters more than species richness in plant community stability at a global scale, Proceedings of the National Academy of Sciences **117**, 24345 (2020).

[47] S. L. Pimm, The complexity and stability of ecosystems, Nature **307**, 321 (1984).

[48] A. R. Ives, J. L. Klug, and K. Gross, Stability and species richness in complex communities, Ecology Letters **3**, 399 (2000).

[49] A. Jousset, W. Schulz, S. Scheu, and N. Eisenhauer, Intraspecific genotypic richness and relatedness predict the invasibility of microbial communities, The ISME journal **5**, 1108 (2011).

[50] C. A. Mallon, J. D. Van Elsas, and J. F. Salles, Microbial invasions: the process, patterns, and mechanisms, Trends in microbiology **23**, 719 (2015).

[51] J. A. Capitán, S. Cuenda, and D. Alonso, Stochastic competitive exclusion leads to a cascade of species extinctions, Journal of Theoretical Biology **419**, 137 (2017).

[52] M. D. Lynch and J. D. Neufeld, Ecology and exploration of the rare biosphere, Nature Reviews Microbiology **13**, 217 (2015).

[53] L. Leidinger and J. S. Cabral, Biodiversity dynamics on islands: Explicitly accounting for causality in mechanistic models, Diversity **9**, 30 (2017).

[54] A. E. Magurran, *Measuring biological diversity* (John Wiley & Sons, 2013).

[55] G. Hardin, The competitive exclusion principle, science **131**, 1292 (1960).

[56] R. MacArthur and R. Levins, The limiting similarity, convergence, and divergence of coexisting species, The american naturalist **101**, 377 (1967).

[57] R. Mac Arthur, Species packing, and what competition minimizes, Proceedings of the National Academy of Sciences **64**, 1369 (1969).

[58] G. F. Gause, *The Struggle for Existence: A Classic of Mathematical Biology and Ecology* (Courier Dover Publications, 2019).

[59] M. Scheffer and E. H. van Nes, Self-organized similarity, the evolutionary emergence of groups of similar species, Proceedings of the National Academy of Sciences **103**, 6230 (2006).

[60] R. Vergnon, E. H. Van Nes, and M. Scheffer, Emergent neutrality leads to multimodal species abundance distributions, Nature communications **3**, 1 (2012).

[61] D. A. Kessler and N. M. Shnerb, Generalized model of island biodiversity, Physical Review E **91**, 042705 (2015).

[62] G. Bunin, Interaction patterns and diversity in assembled ecological communities, arXiv preprint arXiv:1607.04734 (2016).

[63] F. Roy, M. Barbier, G. Biroli, and G. Bunin, Complex interactions can create persistent fluctuations in high-diversity ecosystems, PLoS computational biology **16**, e1007827 (2020).

[64] C. K. Fisher and P. Mehta, The transition between the niche and neutral regimes in ecology, Proceedings of the National Academy of Sciences **111**, 13111 (2014).

[65] W. Verberk, Explaining general patterns in species abundance and distributions, Nature Education Knowledge **3**, 38 (2011).

[66] M. S. Fowler and L. Ruokolainen, Colonization, covariance and colour: Environmental and ecological drivers of diversity–stability relationships, Journal of theoretical biology **324**, 32 (2013).

[67] G. Barabás, M. J. Michalska-Smith, and S. Allesina, The effect of intra-and interspecific competition on coexistence in multispecies communities, The American Naturalist **188**, E1 (2016).

[68] D. Alonso, R. S. Etienne, and A. J. McKane, The merits of neutral theory, Trends in ecology & evolution **21**, 451 (2006).

[69] B. Haegeman and M. Loreau, A mathematical synthesis of niche and neutral theories in community ecology, Journal of theoretical biology **269**, 150 (2011).

[70] G. J. Baxter, R. A. Blythe, and A. J. McKane, Exact solution of the multi-allelic diffusion model, Mathematical biosciences **209**, 124 (2007).

[71] A. J. McKane, D. Alonso, and R. V. Solé, Analytic solution of hubbell's model of local community dynamics, Theoretical Population Biology **65**, 67 (2004).

[72] S. Xu and T. Chou, Immigration-induced phase transition in a regulated multispecies birth-death process, Journal of Physics A: Mathematical and Theoretical **51**, 425602 (2018).

[73] J. A. Capitán, S. Cuenda, and D. Alonso, Competitive dominance in plant communities: Modeling approaches and theoretical predictions, Journal of Theoretical Biology **502**, 110349 (2020).

[74] A. J. Black and A. J. McKane, Stochastic formulation of ecological models and their applications, Trends in ecology & evolution **27**, 337 (2012).

[75] R. MacArthur, Species packing and competitive equilibrium for many species, Theoretical population biology **1**, 1 (1970).

[76] P. Chesson, Macarthur's consumer-resource model, Theoretical Population Biology **37**, 26 (1990).

[77] J. P. O'Dwyer, Whence lotka-volterra?, Theoretical Ecology **11**, 441 (2018).

[78] S. Allesina and S. Tang, Stability criteria for complex ecosystems, Nature **483**, 205 (2012).

[79] C. W. Gardiner *et al.*, *Handbook of stochastic methods*, Vol. 3 (springer Berlin, 1985).

[80] J. Hu, D. Amor, M. Barbier, G. Bunin, and J. Gore, Emergent phases of ecological diversity and dynamics mapped in microcosms (2021).

[81] A. Carr, C. Diener, N. S. Baliga, and S. M. Gibbons, Use and abuse of correlation analyses in microbial ecology, The ISME journal **13**, 2647 (2019).

[82] D. P. Chance, J. R. McCollum, G. M. Street, B. K. Strickland, and M. A. Lashley, Native species abundance buffers non-native plant invasibility following intermediate forest management disturbances, Forest Science **65**, 336 (2019).

[83] R. M. May, Will a large complex system be stable?, Nature **238**, 413 (1972).

[84] S. Allesina and M. Pascual, Network structure, predator–prey modules, and stability in large food webs, Theoretical Ecology **1**, 55 (2008).

[85] G. Bunin, Ecological communities with lotka-volterra dynamics, Physical Review E **95**, 042414 (2017).

[86] A. Weigelt, E. Marquard, V. M. Temperton, C. Roscher, C. Scherber, P. N. Mwangi, S. Von Felten, N. Buchmann, B. Schmid, E.-D. Schulze, *et al.*, The jena experiment: six years of data from a grassland biodiversity experiment, Ecology **91**, 930 (2010).

[87] P. Jeraldo, M. Sipos, N. Chia, J. M. Brulc, A. S. Dhillon, M. E. Konkel, C. L. Larson, K. E. Nelson, A. Qu, L. B. Schook, *et al.*, Quantification of the relative roles of niche and neutral processes in structuring gastrointestinal microbiomes, Proceedings of the National Academy of Sciences **109**, 9692 (2012).

[88] M. Dornelas and S. R. Connolly, Multiple modes in a coral species abundance distribution, Ecology Letters **11**, 1008 (2008).

[89] C. T. Callaghan, S. Nakagawa, and W. K. Cornwell, Global abundance estimates for 9,700 bird species, Proceedings of the National Academy of Sciences **118** (2021).

[90] E. Ser-Giacomi, L. Zinger, S. Malviya, C. De Vargas, E. Karsenti, C. Bowler, and S. De Monte, Ubiquitous abundance distribution of non-dominant plankton across the global ocean, Nature ecology & evolution **2**, 1243 (2018).

[91] T. J. Matthews, P. A. Borges, and R. J. Whittaker, Multimodal species abundance distributions: a deconstruction approach reveals the processes behind the pattern, Oikos **123**, 533 (2014).

[92] T. Oakes, J. M. Heather, K. Best, R. Byng-Maddick, C. Husovsky, M. Ismail, K. Joshi, G. Maxwell, M. Noursadeghi, N. Riddell, *et al.*, Quantitative characterization of the t cell receptor repertoire of naïve and memory subsets using an integrated experimental and computational pipeline which is robust, economical, and versatile, Frontiers in immunology **8**, 1267 (2017).

[93] L. Descheemaeker and S. de Buyl, Stochastic logistic models reproduce experimental time series of microbial communities, Elife **9**, e55650 (2020).

Supplemental materials to the manuscript Phenomenology and Dynamics of Competitive Ecosystems Beyond the Niche-Neutral1 Regimes

APPROXIMATIONS OF SPECIES ABUNDANCE DISTRIBUTION

Derivation of zero flux in n_i - Global balance equation - derivation for the exact SAD

Consider the multi-dimensional master equation

$$\partial_t P(n_1, n_2 \ldots, n_S) = \sum_i \left\{ q_i^+(\vec{n} - \vec{e_i})P(\vec{n} - \vec{e_i}) + q_i^-(\vec{n_i} + \vec{e_i})P(\vec{n} + \vec{e_i}) - \left[q_i^+(\vec{n}) + q_i^-(\vec{n}) \right] P(\vec{n}) \right\} \tag{1}$$

where $q_{n_i}^+(\vec{n})$ and $q_{n_i}^-(\vec{n})$ represents the birth and death rate of species i (respectively), which are generally depends in $\vec{n} = (n_1, \ldots, n_s)$. Here, $e_i = \{0, \ldots, 1, \ldots, 0\}$ (the one is located in the i-th component). To find Master equation for n_1 we sum over all other components; i.e.

$$\sum_{n_2=0}^{\infty} \cdots \sum_{n_s=0}^{\infty} \partial_t P(n_1, n_2 \ldots, n_S) = \tag{2}$$

$$= \sum_{n_2=0}^{\infty} \cdots \sum_{n_s=0}^{\infty} \left\{ \sum_i \left\{ q_i^+(\vec{n} - \vec{e_i})P(\vec{n} - \vec{e_i}) + q_i^-(\vec{n_i} + \vec{e_i})P(\vec{n} + \vec{e_i}) - \left[q_i^+(\vec{n}) + q_i(\vec{n}) \right] P(\vec{n}) \right\} \right\}$$

thus

$$\partial_t P_1(n_1) = \sum_{n_2=0}^{\infty} \cdots \sum_{n_s=0}^{\infty} \left\{ \sum_i \left\{ q_i^+(\vec{n} - \vec{e_i})P(\vec{n} - \vec{e_i}) + q_i^-(\vec{n_i} + \vec{e_i})P(\vec{n} + \vec{e_i}) - \left[q_i^+(\vec{n}) + q_i(\vec{n}) \right] P(\vec{n}) \right\} \right\}. \tag{3}$$

We can now use the fact that for every n_i:

$$\sum_{n_i=0}^{\infty} q_i^+(n_1, \ldots n_i - 1, \ldots, n_S)P(n_1, \ldots n_i - 1, \ldots, n_S) = \sum_{n_i=0}^{\infty} q_i^+(n_1, \ldots n_i, \ldots, n_S)P(n_1, \ldots n_i, \ldots, n_S), \quad \text{and} \tag{4}$$

$$\sum_{n_i=0}^{\infty} q_{n_i}^-(n_1, \ldots n_n + 1, \ldots, n_S)P(n_1, \ldots n_i + 1, \ldots, n_S) = \sum_{n_i=0}^{\infty} q_{n_i}^-(n_1, \ldots n_i, \ldots, n_S)P(n_1, \ldots n_i, \ldots, n_S)$$

[note that $q_{n_i}^+(n_1, \cdots - 1, \ldots, n_S)P(n_1, \ldots, -1, \ldots, n_S) = q_{n_i}^-(n_1, \ldots 0, \ldots, n_S)P(n_1, \ldots 0, \ldots, n_S) = 0$]. Thus, the above equation is given by

$$\partial_t P_1(n_1) = \sum_{n_2=0}^{\infty} \cdots \sum_{n_s=0}^{\infty} \left\{ q_1^+(\vec{n} - \vec{e_1})P(\vec{n} - \vec{e_1}) + q_1^-(\vec{n} + \vec{e_1})P(\vec{n} + \vec{e_1}) - \left[q_1^+(\vec{n}) + q_1^-(\vec{n}) \right] P(\vec{n}) \right\}. \tag{5}$$

For simplicity, we define $F^+(\vec{n}) \equiv q_1^+(\vec{n})P(\vec{n})$ and $F^-(\vec{n}) \equiv q_1^-(\vec{n})P(\vec{n})$, thus Eq. can be written as

$$\partial_t P(n_1) = \sum_{n_2=0}^{\infty} \cdots \sum_{n_s=0}^{\infty} \left\{ F^+(n_1 - 1, n_2, \ldots) - F^+(n_1, n_2, \ldots) + F^-(n_1 + 1, n_2, \ldots) - F^-(n_1, n_2, \ldots) \right\}. \tag{6}$$

By using z-transform $(n_1 \to z)$, which is defined for a function $k(n_1)$ as $K(z) = \sum_{n_1=0}^{\infty} k(n_1)z^{-n_1}$, we obtain

$$\partial_t P(z) = \sum_{n_2=0}^{\infty} \cdots \sum_{n_s=0}^{\infty} F_{\text{right}}(z, n_2, \ldots)(1 - z^{-1}) + F_{\text{left}}(z, n_2, n_3 \ldots)(1 - z) \tag{7}$$

{used $\mathcal{Z}[g(n) - g(n-1)] = [1 - z^{-1}]\hat{G}(z)$, and $\mathcal{Z}[g(n+1) - g(n))] = [1 - z]\hat{G}(z) - zg(0)$ }. Stationary solution; $\partial_t P(z) = 0$ and re-organize the equation yields

$$\sum_{n_2=0}^{\infty} \cdots \sum_{n_s=0}^{\infty} F_{\text{right}}(z, n_2, n_3, \ldots) = \sum_{n_2=0}^{\infty} \cdots \sum_{n_s=0}^{\infty} F_{\text{left}}(z, n_2, n_3, \ldots)\frac{1 - z}{z^{-1} - 1} = \sum_{n_2=0}^{\infty} \cdots \sum_{n_s=0}^{\infty} F_{\text{left}}(z, n_2, n_3 \ldots)z. \tag{8}$$

Then, we use the inverse z-transform $(z \to n_1)$, and find

$$\sum_{n_2=0}^{\infty} \cdots \sum_{n_s=0}^{\infty} q_1^+(\vec{n}) P(\vec{n}) = \sum_{n_2=0}^{\infty} \cdots \sum_{n_s=0}^{\infty} q_1^-(\vec{n} + \vec{e_1}) P(\vec{n} + \vec{e_1}). \tag{9}$$

We use Bayes formula; $P(n_1, n_2, n_3, \ldots, n_S) = P(n_2, n_3, \ldots, n_S|n_1) P(n_1)$ and obtain

$$\langle q_{n_1}^+(\vec{n})|n_1\rangle_{n_2, n_3, \ldots, n_S} P_1(n_1) = \langle q_{n_1}^-(\vec{n} + \vec{e_1})|n_1 + 1\rangle_{n_2, \ldots n_S} P_1(n_1 + 1), \tag{10}$$

where $\langle *|n_1\rangle_{n_2, \ldots, n_S} \equiv \langle *|n_1\rangle \equiv \sum_{n_2=0}^{\infty} \cdots \sum_{n_S=0}^{\infty} (*) P(n_2, \ldots, n_S|n_1)$. Up to now there are no assumption in the derivation, and the above is general. For our case, as specified in the main text, $\langle q_1^+(\vec{n})|n_1\rangle = \mu + r^+ n_1$ (note that q_i^+ depends solely on n_i) and $\langle q_1^-(\vec{n})|n_1\rangle = n_1 \left(r^- + rn_1/K + r\rho \sum_{j\neq 1} \langle n_j|n_1\rangle/K \right)$. Additionally, from symmetry, $P_i(n_i) = P_j(n_j) = P(n)$ for every i, j. Thus, solving the recursive equation and obtain

$$P(n) = P(0) \prod_{n'=1}^{n} \frac{q^+(n'-1)}{\langle q^-(\vec{n})|n'\rangle} = \tag{11}$$

$$= P(0) \prod_{n'=1}^{n} \frac{r^+(n'+a)}{n\left(r^- + rn'/K + r\rho \sum_{j\neq 1} \langle n_j|n'\rangle/K\right)} = P(0) \frac{(r^+)^n (a)_n}{n! \prod_{n'=1}^{n} \left(r^- + rn'/K + r\rho \sum_{j\neq 1} \langle n_j|n'\rangle/K\right)}.$$

where $a = \mu/r^+$ and $(a)_n \equiv a(a+1)\ldots(a+n-1)$, in the Pochhammer symbol. Here, $P(0)$ is given from normalization. We emphasize that the above abundance distribution $P(n)$ in (11) is exact, means no approximations have been taken so far.

Note, that the denominator in the exact solution depends on the effect of interactions from all other species over n_1, through the term $\sum_{j\neq 1} \langle n_j|n_1\rangle$. Therefore, in order to provide an explicit expression to $P_1(n_1)$, we need to use some approximations. Three approximation approaches, and a discussion about their limitations are given in the following subsections. We note that all the presented approximations below provide decent results. However, we find that none of them manage to provide adequate fit for every set of parameters, see Figures.

Approximation Approach I: Estimating $\sum_{j\neq i} \langle n_j|n_i\rangle$ Using Mean-Field Approximation

We assume $\langle n_j|n_i\rangle = \langle n_j\rangle$. Thus,

$$P(n) \approx P(0) \frac{(r^+)^n (a)_n}{n! \prod_{n'=1}^{n} \left(r^- + rn'/K + r\rho \sum_{j\neq 1} \langle n_j\rangle/K\right)} = P(0) \frac{(r^+)^n (a)_n}{n! \prod_{n'=1}^{n} (r^- + rn'/K + r\rho(S-1)\langle n\rangle/K)}, \quad \tag{12}$$

where the last equality is given from symmetry; $\langle n_j\rangle = \langle n_i\rangle = \langle n\rangle$ for every species i, j. In addition, by definition, $\langle n\rangle = \sum_{n=0}^{\infty} nP(n)$, hence

$$\langle n\rangle \approx P(0) \sum_{n=0}^{\infty} n \frac{(r^+)^n (a)_n}{n! \prod_{n'=1}^{n} (r^- + rn'/K + r\rho(S-1)\langle n\rangle/K)} \tag{13}$$

where $P(0) = 1/{}_1F_1[a, b; c]$ is the normalization coefficient, with ${}_1F_1[a, b; c]$ is the Kummer confluent hypergeometric function, $a = \frac{\mu}{r^+}$, $b = \frac{r^- K + r\rho(S-1)\langle n\rangle}{r} + 1$ and $c = \frac{r^+ K}{r}$. Solving numerically the above implicit equation and evaluate $\langle n\rangle$. The last step is to substitute the numerical solution of $\langle n\rangle$, obtained from (13), into (12).

Approximation Approach II: Estimating $\langle J|n\rangle$ using Convolution

The exact solution can be written as

$$P_1(n_1) = P(n) = P(0) \frac{(r^+)^n (a)_n}{n! \prod_{n'=1}^{n} (r^- + r(1-\rho)n'/K + r\rho\langle J|n_1\rangle/K)}, \tag{14}$$

where $J = \sum_{i=1}^{\infty} n_i$ is the total population size. Here we assume that the total number of individuals in the system, J, is weekly depends on n_1. Thus J is an independent random variable. Hence,

$$P_1(n_1) = P(n_1|\langle J|n_1\rangle) \approx P(n_1|J) = P(0)\frac{(a)_{n_1}\tilde{c}^{n_1}}{n_1!(\tilde{b}+1)_{n_1}} \tag{15}$$

with $a = \frac{\mu}{r^+}$, $\tilde{b} = \frac{r^- K + r\rho J}{r(1-\rho)}$, and $\tilde{c} = \frac{r^+ K}{r(1-\rho)}$ [note that both $\tilde{b}$ and $\tilde{c}$ differ from b and c defined in previous subsection]. Moreover, we assume that the species levels are mutually independent, means $\mathcal{P}(n_1,\dots n_S) \approx \prod_i P_i(n_i)$. Thus, the PDF of $\sum_i n_i$ reads

$$P\left(\sum_i n_i \middle| J\right) = \underbrace{P_1(n_1|J) * P_2(n_2|J) * \cdots * P_S(n_S|J)}_{S \text{ times}} \tag{16}$$

where $A * B$ means the convolution of A with B. $P\left(\sum_i n_i | J\right)$ is the 'analytical' PDF to have $\sum_i n_i$ individuals where we assume that a single species PDF is $P_1(n_1|J)$ with a given J. To capture the fact that J has a meaning of number of individuals as well, we consider

$$P(J) \approx \frac{\text{Prob}\left(\sum_i n_1 = J| J\right)}{\sum_J \text{Prob}\left(\sum_i n_1 = J| J\right)}, \tag{17}$$

where $P(J)$ is the approximated distribution of J. Then

$$P_1(n_1) = \sum_J P_1(n_1|J)P(J) \tag{18}$$

is the approximated PDF.

Note that when S is large, we find

$$P\left(\sum_i n_i \middle| J\right) \sim \mathcal{N}\left(S\langle n_1|J\rangle, S \cdot Var(n_i)\right), \tag{19}$$

thus $P(J) \approx \text{Prob}(\sum_i n_i = J|J)$ reaches its maximum in the vicinity of J which satisfies $J \approx S\langle n_i|J\rangle = \langle\sum_i n_i|J\rangle$. Furthermore, for the approximation $P(J) \approx \text{Prob}(\sum_i n_i = J|J)$, the values of J where $J \ll S\langle n_i|J\rangle$ or $J \gg S\langle n_i|J\rangle$ are highly improbable, due to the Gaussian nature of $P(\sum_i n_i|J)$ for large S.

Approximation Approach III: Estimating $\langle J|n\rangle$ using Mean-Field Approximation

In a similar fashion to previous approximation approaches, we assume $\langle J|n\rangle \approx \langle J\rangle$, thus

$$P(n) \approx P(0)\frac{(r^+)^n(a)_n}{n!\prod_{n'=1}^n (r^- + r(1-\rho)n'/K + r\rho\langle J\rangle/K)} = P(0)\frac{(r^+)^n(a)_n}{n!\prod_{n'=1}^n (r^- + r(1-\rho)n'/K + r\rho S\langle n\rangle/K)}. \tag{20}$$

Then, $\langle n\rangle$ is given by the numerical solution of

$$\langle n\rangle = \sum_{n=0}^{\infty} nP(0)\frac{(r^+)^n(a)_n}{n!\prod_{n'=1}^n (r^- + r(1-\rho)n'/K + r\rho S\langle n\rangle/K)}. \tag{21}$$

where here the normalization factor is $P(0) = 1/_1F_1[a,b;c]$ with $a = \frac{\mu}{r^+}$, $\tilde{\tilde{b}} = \frac{r^- K + r\rho\langle J\rangle}{r(1-\rho)}$, and $\tilde{c} = \frac{r^+ K}{r(1-\rho)}$.

Interspecies Correlations and Limitations of the Approximations Approaches

For approximation approaches described above, we assume the species are mutually independent, meaning $P(\vec{n}) = \prod_{i=1}^S P(n_i)$. Of course, this mutual independence cannot exactly be obtained, except for $\rho = 0$, since for every $\rho > 0$ the dynamics of a species, i.e its birth and death rates, depends on other species levels. Therefore, we
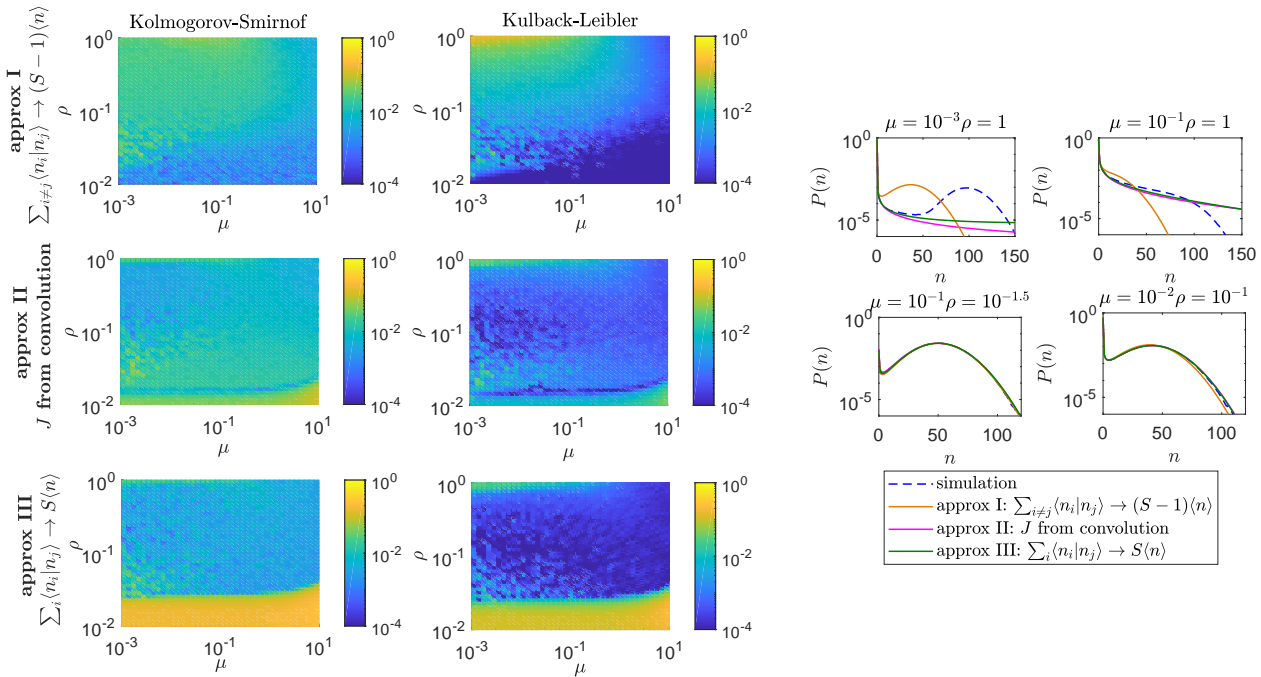
FIG. 1. Quality of Approximation

expect deviations of our approximation from the true simulated SAD. In particular, we expect a relation between the interspecies correlation and the quality of approximation.

We quantify the quality of approximation, using two metrics. The first one, Kolmogorov-Smirnov (KS), is defined with $KS(P,Q) \equiv \max |\text{CDF}(P) - \text{CDF}(Q)|$ for two PDFs, P and Q. The second metric we use is the Kullback–Leibler divergence, which is defined by $KL(P,Q) \equiv \sum_x (P-Q) \ln (P/Q)$. Intuitively, the KS metric captures the difference between the approximation and the simulation results, and the KL divergence capture the ratio between the distributions. Fig. 1 shows the KS and KL metrics comparing the three approximations presented above and the simulation results.

In the main text, we choose to present the results for the regime boundaries obtained from the Approximation I above. Even so, all approximations present reasonable agreement with the simulation. However, in some regimes, some approximations work better than the others. Additionally, one approximation may better capture some features of the system, while other approximation show better agreement with other features. For example, only approximation (I) captures the bi-modality at very low μ and $\rho = 1$, where the other approximations seem to align with the simulated SAD slightly better.

Tail-end of distributions

The above model does not describe an ecological zero-sum game as the total population size $J = \sum_i n_i$ may fluctuate in this proposed formulation. Conversely, classical Moran models describe stochastic processes in which the finite population is fixed. The species abundance distribution can be solved for exactly in certain cases where this assumption of a fixed total population size holds.

In this limit,

$$P(n) = P(0)\frac{(a)_n}{n!} \approx P(0)\frac{n^{a-1}}{\Gamma[a]} \tag{22}$$

In the case where $\langle J|n_1\rangle \approx \langle J\rangle$:

$$P(n) = P(0)\left(\frac{r^+}{r^- + r\langle J\rangle/K}\right)^n \frac{(a)_n}{n!} \approx P(0)\left(\frac{r^+}{r^- + r\langle J\rangle/K}\right)^{n_1} \frac{n_1^{a-1}}{\Gamma[a]}. \tag{23}$$

Note that this is valid only when $n \gg a$, that is to say for the tail-end of the distributions.

Moran models are generally neutral $\rho = 1$), however using our demographic noise model allows for observing non-neutral systems. We can approximate the tail of the distribution for non-neutral models ($0 < \rho < 1$) using similar arguments as above, that is to say approximating $\langle J|n\rangle \approx J$. Using our previous solution and this approximation, we find that

$$P(n) = P(0)\frac{(r^+)^n(a)_n}{n!\prod_{n'=1}^n(r^- + r(1-\rho)n'/K + \rho\langle J|n'\rangle/K)} \approx P(0)\frac{(a)_n\tilde{c}^n}{n!(\tilde{b}+1)_n} \tag{24}$$

where $a = \frac{\mu}{r^+}$, $\tilde{b} = \frac{r^-K+r\rho J}{r(1-\rho)}$, and $\tilde{c} = \frac{r^+K}{r(1-\rho)}$. Looking at the tail of the distribution ($n \gg a, \tilde{b}, \tilde{c}$) we find that

$$P(n) \xrightarrow{n\to\infty} P(0)\frac{\Gamma[\tilde{b}+1]}{\sqrt{2\pi}\Gamma[a]}n^{a-\tilde{b}-\frac{3}{2}}(\tilde{c}/n)^n e^n \tag{25}$$

where we have used Stirling's approximation that $n! \approx \sqrt{2\pi n}n^n e^{-n}$. In the high n limit, we can further approximate $J \sim n$ such that $P(n) \sim n^{-n/(1-\rho)}e^n$

In the case where $\rho \to 0$, there is no need for approximating $\langle J|n\rangle$, as that term disappears in the exact solution. We are left with the solution

$$P(n) \xrightarrow{\rho\to 0} P(0)\frac{(\mu/r^+)_n(r^+K/r)^n}{n!(r^-K/r+1)_n} \tag{26}$$

which is exact. The tail of this distribution goes as

$$P(n) \xrightarrow{\rho\to 0, n\to\infty} P(0)\frac{\Gamma[r^-\tilde{K}/r+1]}{\sqrt{2\pi}\Gamma[\mu/r^+]}n^{\frac{\mu}{r^+}-\frac{r^-K}{r}-\frac{3}{2}}(r^-K/rn)^n e^n. \tag{27}$$

Note that the denominator of $\tilde{b}$ and $\tilde{c}$ goes to 0 as $\rho \to 1$, as such the limit must be taken carefully: $\tilde{b} \xrightarrow{\rho\to 1} \infty$. We use the fact that $(x+1)_n \xrightarrow{x\to\infty} x^n$ to write

$$P(n) \xrightarrow{\rho\to 1} P(0)\frac{(a)_n\{r^+K/[r(1-\rho)]\}^n}{n!\{(r^-K+rJ)/[r(1-\rho)]\}^n} = P(0)\frac{(a)_n(r^+K)^n}{n!(r^-K+rJ)^n} \xrightarrow{n\to\infty} P(0)\left(\frac{r^+K}{r^-K+rJ}\right)^n \frac{n^{a-1}}{\Gamma[a]} \tag{28}$$

which agrees with what we found earlier for $\rho = 1$ and constant J. For $\rho = 1$, we know that if any one species abundance gets large it should dominate the system. Therefore, we can approximate $J \approx n$ for large n in the neutral regime.

This asymptotic behaviour may be compared to analytical solutions for which J is held constant. These Moran type models are often solvable exactly, we choose to show their results wherein $J = Sn_{det}$ where n_{det} is the solution to the mean deterministic equation Lotka-Voltera equation. In [1], an analytical solution to the Hubbel model with immigration is found such that

$$P(n) = \binom{J}{n}\frac{\beta(n+p, n^*-n)}{\beta(p^*, n^*-J)} \tag{29}$$

where $p = 1/S$, $n^* = (J-m)/(1-m)-p$, and $p^* = mp(J-1)/(1-m)$. In this model, m is defined as the probability of immigration at any step. This is different from our immigration rate, however we find a suitable transformation to be $m \approx \mu/\langle r_n^+ + r_n^-\rangle$: the probability of immigration is the rate of immigration divided by the mean rate of a reaction. Note that the function $\beta(a,b) = \Gamma(a)\Gamma(b)/\Gamma(a+b)$.

In [2], a continuum Fokker-Planck equation is solved to evaluate a similar multi-allelic diffusion model abundance. However, in this formalism, immigration is replaced by mutations wherein u_i is the rate of mutation of cell allele i. Assuming all the mutation rates are equivalent, $u_i = u$ The steady state joint probability distribution is

$$P(\vec{x}) = \Gamma(2Su)\delta(1 - \sum_i x_i)\prod_{i=0}^{S}\frac{x_i^{2u-1}}{\Gamma(2u)} \tag{30}$$

which may be integrated to find the SAD

$$SAD(n) = \langle\sum_j \delta(x_j - n/J)\rangle_{P(\vec{x})} \approx \left(\frac{n}{J}\right)^{2u-1}e^{-(2u(S-1)-1)n/J} \tag{31}$$

Although mutations and immigration are not completely equivalent, mutations may take on a heuristic role similar to immigration that allows for no species to be truly extinct. As such, we assume $u = \mu/r$. Comparisons of these different asymptotic behaviours are found in Fig. 2.
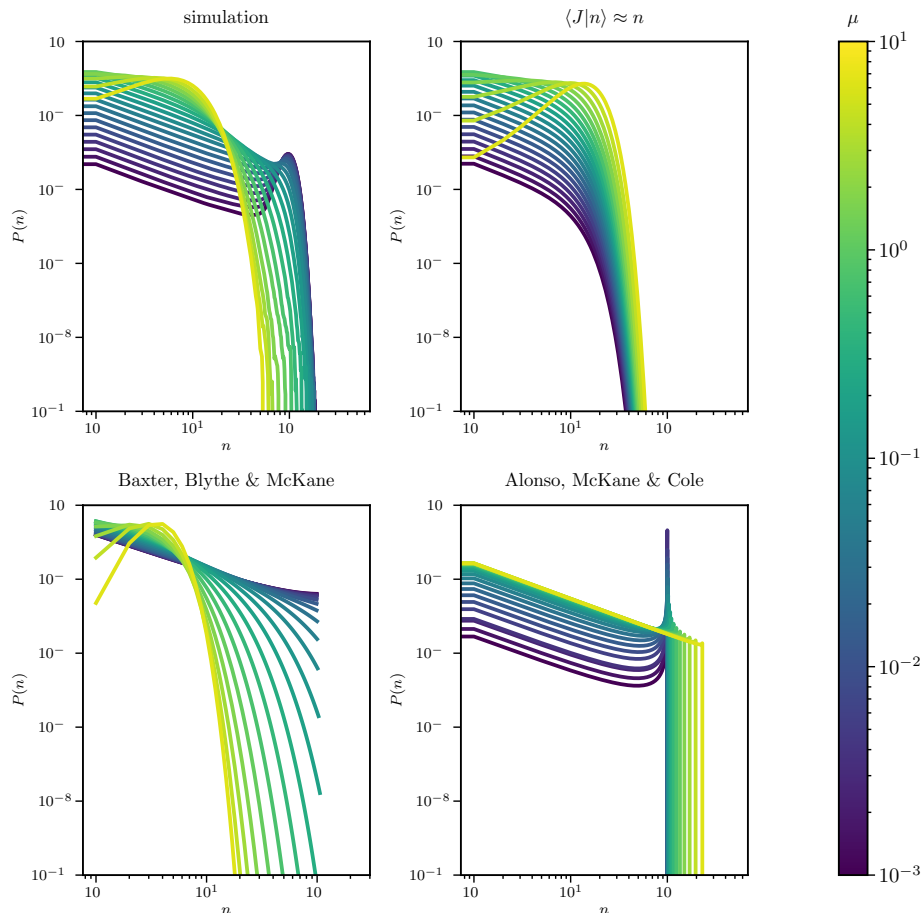

FIG. 2. Asymptotic behaviour of various neutral models compared to simulations. (top panels) Using $\langle J|n\rangle \approx n$, our approximation does not recover a bimodality, however the analytical approximation clearly follows the simulation's power law with exponential cutoff. (bottom panels) Moran-like models in the literature of power-law SADs with exponential cutoff. Here, the total population size used is the total population size of the steady-state Lotka-Voltera equation, $J = Sn_{LV}$. The continuous Fokker-Planck diffusion model of Baxter, Blythe & McKane[2] shows the immigration dominated peak. However, the Hubbel community model solved by Alonso, McKane & Sole[1] shows a bimodality in the low immigration regime. Both have power laws with exponential cutoff in different regimes.

DERIVATIONS OF BOUNDARY EQUATIONS

Boundaries for Richness Regimes

For the boundaries defined from richness, we use $\langle S^* \rangle = S(1 - P(0))$, where $P(0)$ obtained numerically from the approximated SAD. Note that in the mean-filed approximations $P(0)$ is explicitly given as Kummer confluent hypergeometric function. Then, the transition between full richness to partial coexistence is given with $SP(0) = 1/2$ (as the arithmetic mean between the two boundaries). Similarly, the transition boundary between partial coexistence and excluded regime is drawn where $SP(0) = S - 3/2$.

Derivation of $\tilde{n}$

The boundaries defined by the modalities can be given directly from the above approximations, see Figures. However, we have found that using the mean-field approximation allows us to derived a closed expression for the boundaries.

The transition between neutral-like to bimodal regimes, is defined by the presence or absence of a local maximum in a real positive level. In another words, in the neutral-like regime $P(n) > P(n + 1)$, since the SAD is monotony decreasing, while in the bimodal regime, there is $n > 0$ where $P(n) < P(n + 1)$. Thus the boundary between the regimes occurs where

$$P(n) = P(n + 1). \tag{32}$$

Using the $P(n)$ from the mean-field approximation, we find

$$P(0)\frac{(a)_n c^n}{n!(b + 1)_n} = P(0)\frac{(a)_{n+1} c^{n+1}}{(n + 1)!(b + 1)_{n+1}} \tag{33}$$

$$\frac{(b + 1)_{n+1}(n + 1)!}{n!(b + 1)_n} = \frac{(a)_{n+1} c^{n+1}}{(a)_n c^n} \tag{34}$$

$$n(b + n) = c(a + n - 1) \tag{35}$$

$$n = \frac{(c - b) \pm \sqrt{(c - b)^2 + 4(a - 1)c}}{2} \tag{36}$$

Substitute $a = \frac{\mu}{r^+}$, $b = \frac{r^- K + r\rho(S - 1)\langle n \rangle}{r} + 1$ and $c = \frac{r^+ K}{r}$ yields

$$\tilde{n} \approx \frac{K - \rho(S - 1)\langle n \rangle}{2}\left\{1 \pm \sqrt{1 + 4\frac{(\mu - r^+)K}{r(K - \rho(S - 1)\langle n \rangle)^2}}\right\}. \tag{37}$$

If we use $S\langle n \rangle = \langle S^* \rangle \tilde{n}$, we find

$$\tilde{n} = \frac{K}{2(1 - \rho + \rho\langle S^* \rangle)}\left\{1 + \sqrt{1 + \frac{4(\mu - r^+)(1 - \rho + \rho\langle S^* \rangle)}{rK}}\right\} \approx \frac{K}{1 - \rho + \rho\langle S^* \rangle} - \frac{\mu - r^+}{r}. \tag{38}$$

Boundaries for Modalities Regimes

In the neutral-like regime the SAD is monotonously decreasing. Therefore, the neutral-like regime is sufficiently define by either imaginary $\tilde{n}$, or real but negative $\tilde{n}$. The transition line between real and imaginary $\tilde{n}$, i.e. where $\Im(\tilde{n}) = 0$, is given by

$$r\left[K - \rho(S - 1)\langle n \rangle\right]^2 = 4(r^+ - \mu)K. \tag{39}$$

The transition line between the negative to positive $\tilde{n}$, where $\tilde{n} = 0$, is drawn where

$$\frac{(K - \rho(S - 1)\langle n \rangle)^2}{4} = 1 + \frac{4K(\mu - r^+)}{r(K - \rho(S - 1)\langle n \rangle)^2}. \tag{40}$$

Therefore, the neutral-like regime is defines as the union of the regions defined by both two equations above.

The second boundary we derive is the border of uni-modality region with positive probable abundance. At zero abundance, the abundance distribution poses either local maximum ($P(0) > P(1)$; correspond to bimodality or neutral-like regimes) or local minimum ($P(0) < P(1)$; unimodality). Consequently, the boundary between these two possibilities is given by $P(0) = P(1)$. Thus, following the zero-flux equation, we obtain

$$q^+(0) = \langle q^-(\vec{n})|1\rangle \implies \mu = r^- + \frac{r}{K}\left[1 - \rho + \rho\langle J\rangle\right]. \tag{41}$$

DEPENDENCE ON CARRYING CAPACITY K

The regime boundaries depend on the carrying capacity, as can be seen in Fig. 3; as the carrying capacity increases, the 'neutral-like' regime shrinks in size. We also find that the full richness regime extends to larger competitive overlap, intuitively suggesting that interspecies competition is decreased in the larger carrying capacity regimes. The larger carrying capacity allows for more individual species to immigrate into the system and coexist.
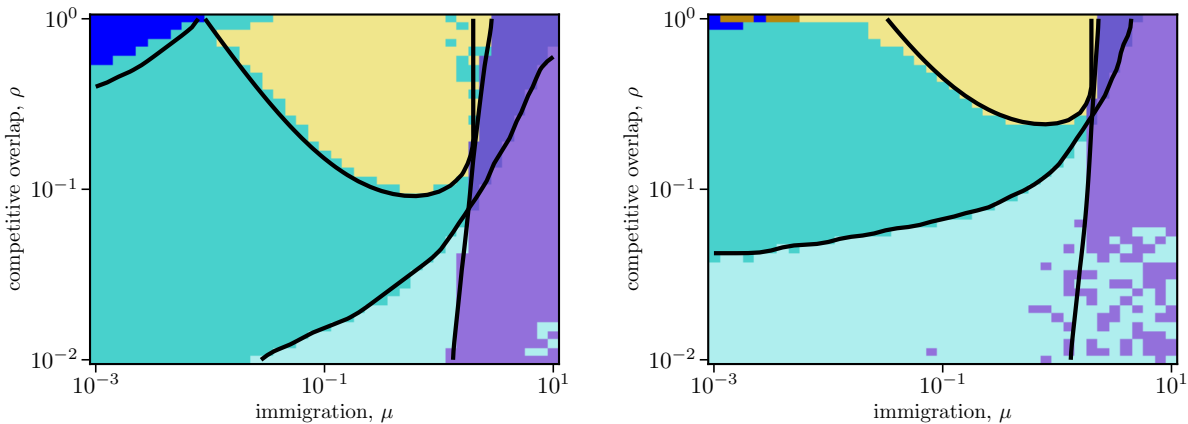

FIG. 3. Varying carry capacity. Left panel: $K = 50$. Right panel: $K = 200$. Note that the the erroneous classification in certain regimes is due to numerical difficulty in determining optima of the SAD.

KINETICS

As was mentioned in the main text, we concentrate on time scales associated with mean-first-passage-time (MFPT) from some initial abundance i, to a final one f. This MFPT, denoted as $\langle T(i \to f)\rangle$, is inversely proportional to the transition rate from i to j, where the first-passage times are exponentially distributed (see Figures). In a unidimensional process in an interval $[0, \infty)$, the MFPTs we consider are

$$\langle T(\tilde{x} \to 0)\rangle = \sum_{y=0}^{\tilde{x}-1} \frac{1}{q^+(y)P(y)} \sum_{z=y+1}^{\infty} P(z), \langle T(0 \to 0)\rangle = \frac{1}{q^+(0)P(0)} = \frac{1}{\mu P(0)}, \tag{42}$$

$$\langle T(0 \to \tilde{x})\rangle = \sum_{y=0}^{\tilde{x}} \frac{1}{q^+(y)P(y)} \sum_{z=0}^{y} P(z), \langle T(\tilde{x} \to \tilde{x})\rangle = \frac{1}{P(\tilde{x})[q^+(\tilde{x}) + q^-(\tilde{x})]}.$$

These expressions are exact for processes in one dimension [3], i.e. for a single species were no other species affect its dynamics. Here we have found, using simulation, that these MFPTs agree with the multi-dimensional scenario, where many species evolve (see Figures). Hence, we substitute the SAD obtained from simulation, as $P(n)$ in the expressions above and estimated the rates with $R(a \to b) = 1/\langle T(a \to b)\rangle$. A similar approach is used to estimate the other rate ratio.
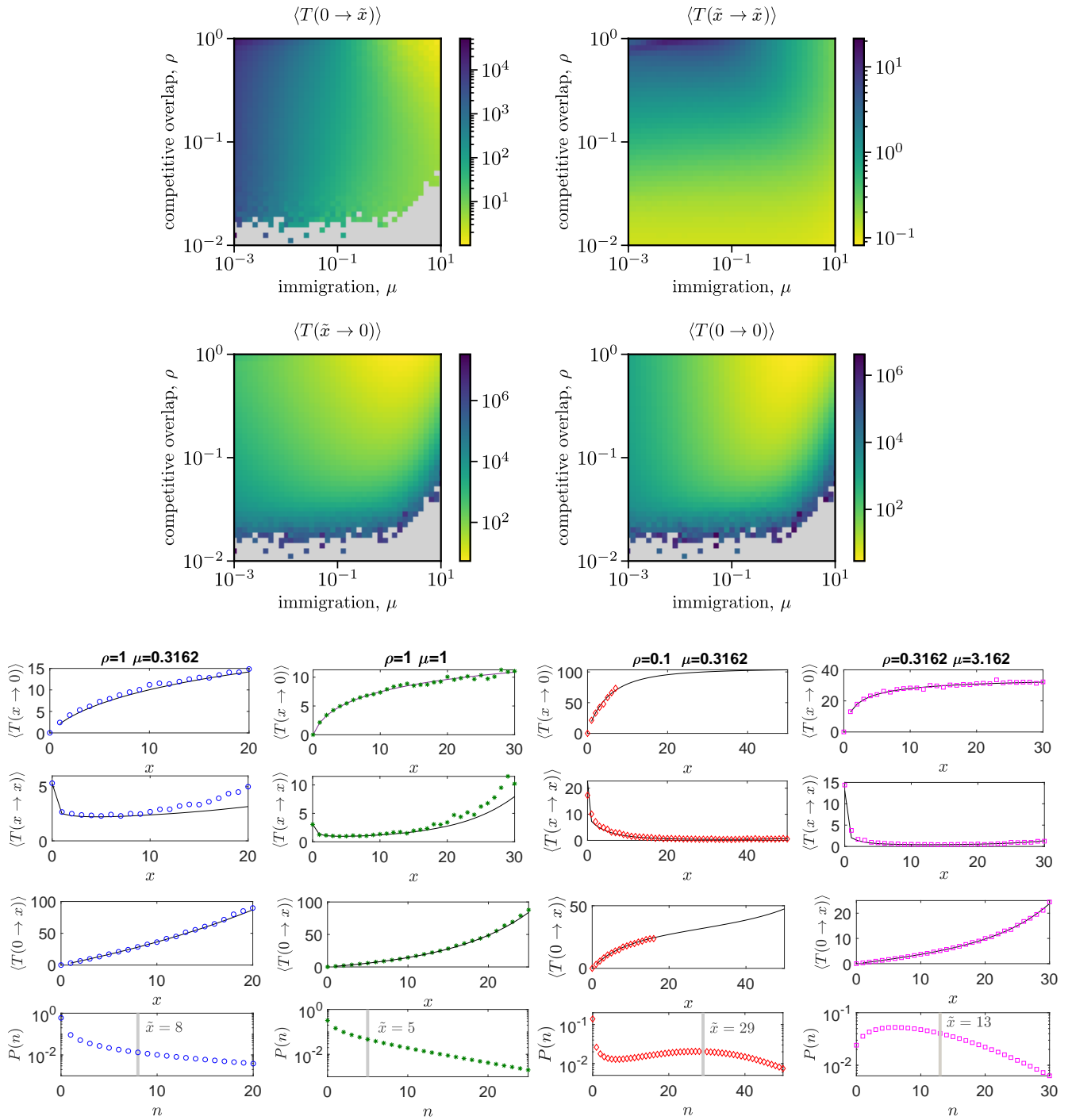
FIG. 4. Turnover time statistics

FOKKER-PLANCK FORMULATION

In the analysis so far we have used n_i to represent a discrete variable, however we may approximate the master equation in a continuum should some large characteristic system size exist. Assuming here that $K >> 1$ is the system size, we define x_i to be the corresponding continuous limit of n_i. The variable may be rescaled by the characteristic system size, $y_i = x_i/K$ This continuous approximation has as probability density $P(\vec{n}, t) = p(\vec{y}, t)/K$ and we may

write the the scaled rates as $q_i^{+/-}(\vec{n}) = KQ_i^{+/-}(\vec{y})$ where

$$Q_i^+(\vec{y}) = r^+ y_i + \mu/K$$

$$Q_i^+(\vec{y}) = r^- y_i + r y_i \left(y_i + \sum_{j \neq i} \rho_{j,i} y_j \right)$$

is defined on the continuum. Then we can write the corresponding master equation as

$$\partial_t p(\vec{x}; t) = K \sum_i \left\{ Q_i^+(\vec{y} - \vec{e}_i) p(\vec{y} - \vec{e}_i, t) + Q_i^-(\vec{y} + \vec{e}_i) p(\vec{y} + \vec{e}_i, t) - \left[Q_i^+(\vec{y}) + Q_i^-(\vec{y}) \right] p(\vec{y}, t) \right\} \tag{43}$$

wherein $\vec{e}_i$ is the change in abundance $\vec{y}$ from the respective event, which in our single birth-death process will be $\vec{e}_i = (\delta_{1i}/K, \delta_{2i}/K, ..., \delta_{Si}/K)$, in other words a vector of zeros except for $1/K$ located at species i. To go from the master equation to the Fokker-Planck equation, we Taylor expand each of the expressions from the right-hand side of 43. As such,

$$Q_i^+(\vec{y}-\vec{e}_i) p(\vec{y}-\vec{e}_i, t) = Q_i^+(\vec{y}) p(\vec{y}, t) + \sum_j (-(\vec{e}_i)_j) \frac{\partial}{\partial y_j} \left(Q_i^+(\vec{y}) p(\vec{y}, t) \right) + \frac{1}{2!} \sum_j \sum_k (\vec{e}_i)_j (\vec{e}_i)_k \frac{\partial^2}{\partial y_j \partial y_k} \left(Q_i^+(\vec{y}) p(\vec{y}, t) \right) + ...$$

$$Q_i^-(\vec{y}+\vec{e}_i) p(\vec{y}+\vec{e}_i, t) = Q_i^-(\vec{y}) p(\vec{y}, t) + \sum_j (\vec{e}_i)_j \frac{\partial}{\partial x_j} \left(Q_i^-(\vec{y}) p(\vec{y}, t) \right) + \frac{1}{2!} \sum_j \sum_k (\vec{e}_i)_j (\vec{e}_i)_k \frac{\partial^2}{\partial y_j \partial y_k} \left(Q_i^-(\vec{y}) P(\vec{y}, t) \right) + ...$$

Note that $(\vec{e}_i)_j = \delta_{ij}/K$ in our single birth-death event process, which simplifies these equations considerably. Now, replacing these expressions in our master equation 43, we note that we can write our equation in orders of $1/K$. Thus, we obtain

$$\partial_t p(\vec{y}; t) = -\sum_j \frac{\partial}{\partial y_j} \left[\left(Q_i^+(\vec{y}) - Q_i^-(\vec{y}) \right) p(\vec{y}, t) \right] + \frac{1}{2K} \sum_j \frac{\partial^2}{\partial y_j \partial y_k} \left[\left(Q_i^+(\vec{y}) + Q_i^-(\vec{y}) \right) p(\vec{y}, t) \right] + \mathcal{O}(1/K^2). \tag{44}$$

Up to order $1/K$, 44 is the Fokker-Planck Equation (FPE) of the process. Using Ito's prescription for SDEs, this corresponds to the Langevin equation

$$dy_i = \left(Q_i^+(\vec{y}) - Q_i^-(\vec{y}) \right) dt + \sqrt{\frac{Q_i^+(\vec{y}) + Q_i^-(\vec{y})}{K}} dW_i \tag{45}$$

where W_i is a standard Wiener process. By multiplying both sides of this equation by the characteristic size $K dy_i = dx_i$,

$$dx_i = \left(q_i^+(\vec{x}) - q_i^-(\vec{x}) \right) dt + \sqrt{K \left(q_i^+(\vec{x}) + q_i^-(\vec{x}) \right)} dW_i \tag{46}$$

where the force term in the Langevin equation recovers the Lotka-Voltera equation.

In particular, a common choice is for the diffusion term to be proportional to the square root of the abundance, such that the noise is independent of other species abundances, as in

$$dx_i = \left(q_i^+(\vec{x}) - q_i^-(\vec{x}) \right) dt + \sqrt{K r x_i} dW_i. \tag{47}$$

However not all choice of birth and death rate appropriately recovers this form.

Using an Euler integration method, simulations of the Langevin equation assess how well the Fokker-Planck approximates the SAD. We find that the Fokker-Planck approximation does not reproduce the complete phase space of the modality regimes for either noise specified in (46) and (47), see Fig. 5. In both cases, the 'neutral-like' regime at high competitive overlap ($\rho > 2 \cdot 10^{-1}$) is present even at low immigration such that no bimodality is observed on the neutral manifold ($\rho = 1$). The boundary between the immigration dominated unimodal regime and other regimes is recovered; in this regime, few fluctuations arise that are sufficiently strong enough to bring any species close to the excluded state, $x_i = 0$. Note that the force term is always positive for some $x_i > 0$, which implies that species will assuredly be deterministically pushed back from exclusion. Additionally, the multimodal regime is absent in all Langevin results.
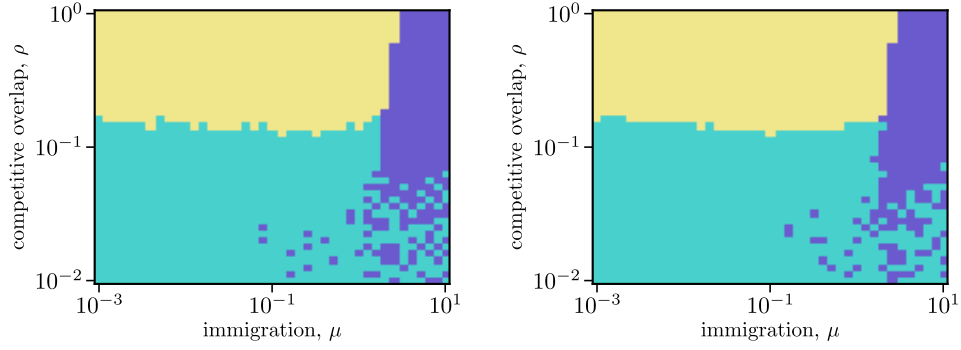
FIG. 5. Langevin numerical simulations. Left: Modality regimes with noise (46) from the rates defined in the main text. Right: Modality regimes with $\sqrt{n}$ noise as in (47). Colours correspond to the modality regime presented in the main text: yellow is the 'neutral-like' regime, teal is the bimodal regime and purple is the immigration dominated unimodal regime.

SPECIES RANK ABUNDANCES VS SPECIES ABUNDANCE DISTRIBUTION

In the vast majority of the manuscript we use species abundance distributions (SADs), together with some dynamical properties, in order to examine and classify processes into deferment regimes. However, in many experimental studies, the species rank abundances (SRAs) are frequently reported instead, e.g see [4–8]. The SRA is closely related to the cumulative distribution correspond to SAD, as is described in the following. First, the cumulative abundance distribution is computed with $\mathrm{CAD}(n) \equiv \sum_0^n P(n')$. Then, we note that the most abundance species, namely species with rank 1, has abundance between $\mathrm{CAD}^{-1}(1 - 1/S)$ to $\mathrm{CAD}^{-1}(1)$. The second most abundance species, i.e. the ranked 2, has abundance between $\mathrm{CAD}^{-1}(1 - 2/S)$ to $\mathrm{CAD}^{-1}(1 - 1/S)$, and so on. Therefore, the x-axis in Fig. 6 is computed with $1 + S(1 - \mathrm{CAD}(n))$ and the y-axis are the abundances n. Using this approach, we generated the SRAs correspond to SAD, see Fig. 6 for the results for $\rho = 1$. However, as is shown in Fig. 6, classification through the SRAs is less significant.
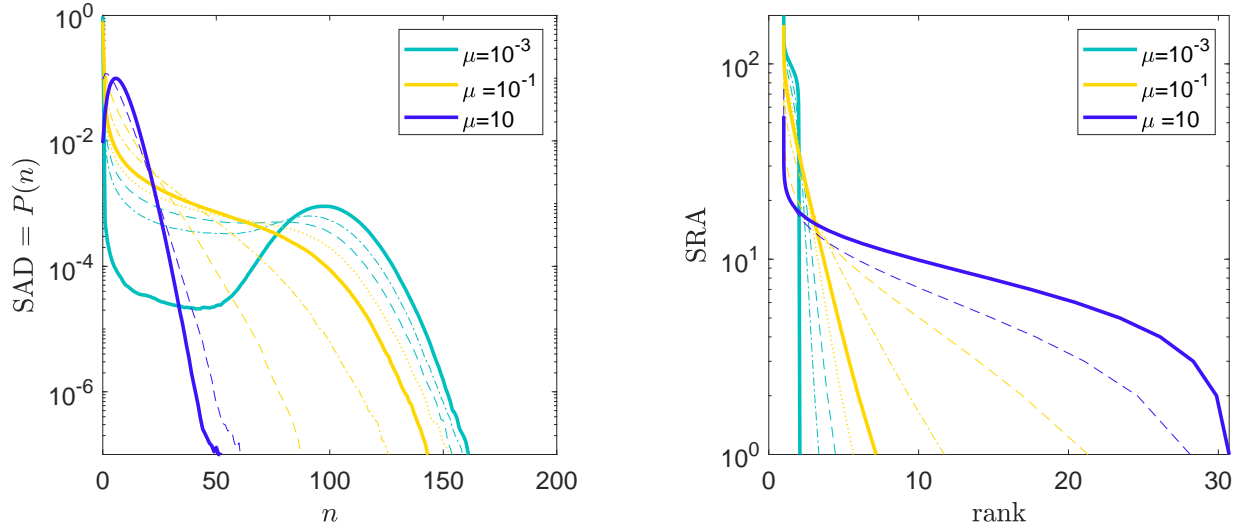

FIG. 6. A comparison between the species abundance distribution (left panel) and its corresponding species rank abundances (right panel). Here $\rho = 1$ is fixed, and the immigration rate μ varies. Solid lines represent $\mu \in [10^{-3}, 10^{-1}, 10]$ following the legend. The dashed, dotted and dashed-dotted lines are in-between μ-s. The color scheme corresponds the modality classification of SAD; teal (bimodal, very low μ), yellow (rare-biosphere, intermediate mu) and blue (unimodal, high μ).

EXPERIMENTAL STUDIES

System (Ref.)	Regimes	Conclusions	Observations
Microbial competition [9]	Stable full coexsitence (IIa), stable partial coexistnce (IIb), persisnt fluctuation (IIIb)	Positive correlation between species and instability (rapid fluctuations)	Community composition/ richness/ fluctuating communities
Global birds species [10]	Unimodal - log skew		SAD
Plankton [4]	Abundance is power-law decay , neutral-like		SAD and SRA
Coral [11]	Multimodal distribution	SAD Not from habitat preferences, most likely due to spatial effects. Common of large samples	SAD
Lymphocyte repertoire [5]	Power law distributions	Functional repertoire is more relevant than actual repertoire, overlap in antigen coverage reduces size for repertoire	SRA
Arthropods [12]	Multi-modal distribution	Propose that multiple modes come from ecologically distinct communities	SAD
Trees [6]	Power law distributions	Different forest types show curves with different slopes, explained by random walk model	SRA
Bacteria [13]	Increasing K, related to Species Area Relation (SAR)	Larger islands have more bacteria taxa on them (increased diversity)	Diversity per islands size
T-cell receptors [14]	Bimodal and unimodal (exponential)	Although total population (CD8 naive cells) has bimodal distirbution, subpopulations have exponential clonotype	SAD
Microbial competition [7]	Neutral-like and niche-like	Heavy tailed rank abundance (microbiome tongue seems to have 2 slopes). Model with linear (extrinsic noise) reproduces this	SRA and time series
Competition in gastrointestinal microbiomes [8]	Non-neutral (niche)	The species abundance patterns are seemingly well fit by the neutral theory, however the operational taxonomic units (OTUs) classify it as niche	SRA and OTUs

TABLE I. Experimental studies consider competitive species and their reported results.

[1] A. J. McKane, D. Alonso, and R. V. Solé, Analytic solution of hubbell's model of local community dynamics, Theoretical Population Biology **65**, 67 (2004).

[2] G. J. Baxter, R. A. Blythe, and A. J. McKane, Exact solution of the multi-allelic diffusion model, Mathematical biosciences **209**, 124 (2007).

[3] C. W. Gardiner *et al.*, *Handbook of stochastic methods*, Vol. 3 (springer Berlin, 1985).

[4] E. Ser-Giacomi, L. Zinger, S. Malviya, C. De Vargas, E. Karsenti, C. Bowler, and S. De Monte, Ubiquitous abundance distribution of non-dominant plankton across the global ocean, Nature ecology & evolution **2**, 1243 (2018).

[5] T. Mora and A. M. Walczak, Quantifying lymphocyte receptor diversity, in *Systems Immunology* (CRC Press, 2018) pp. 183–198.

[6] S. P. Hubbell, Tree dispersion, abundance, and diversity in a tropical dry forest, Science **203**, 1299 (1979).

[7] L. Descheemaeker and S. de Buyl, Stochastic logistic models reproduce experimental time series of microbial communities, Elife **9**, e55650 (2020).

[8] P. Jeraldo, M. Sipos, N. Chia, J. M. Brulc, A. S. Dhillon, M. E. Konkel, C. L. Larson, K. E. Nelson, A. Qu, L. B. Schook, *et al.*, Quantification of the relative roles of niche and neutral processes in structuring gastrointestinal microbiomes, Proceedings of the National Academy of Sciences **109**, 9692 (2012).

[9] J. Hu, D. Amor, M. Barbier, G. Bunin, and J. Gore, Emergent phases of ecological diversity and dynamics mapped in microcosms (2021).

[10] C. T. Callaghan, S. Nakagawa, and W. K. Cornwell, Global abundance estimates for 9,700 bird species, Proceedings of the National Academy of Sciences **118** (2021).

[11] M. Dornelas and S. R. Connolly, Multiple modes in a coral species abundance distribution, Ecology Letters **11**, 1008 (2008).

[12] T. J. Matthews, P. A. Borges, and R. J. Whittaker, Multimodal species abundance distributions: a deconstruction approach reveals the processes behind the pattern, Oikos **123**, 533 (2014).

[13] T. Bell, D. Ager, J.-I. Song, J. A. Newman, I. P. Thompson, A. K. Lilley, and C. J. Van der Gast, Larger islands house more bacterial taxa, Science **308**, 1884 (2005).

[14] T. Oakes, J. M. Heather, K. Best, R. Byng-Maddick, C. Husovsky, M. Ismail, K. Joshi, G. Maxwell, M. Noursadeghi, N. Riddell, *et al.*, Quantitative characterization of the t cell receptor repertoire of naïve and memory subsets using an integrated experimental and computational pipeline which is robust, economical, and versatile, Frontiers in immunology **8**, 1267 (2017).